Raman Spectroscopic Investigation of Porcine Lens Proteins Before and After Ultraviolet Radiation

Thesis

Presented in Partial Fulfillment of the Requirements for the Degree Master of Science in the Graduate School of The Ohio State University

By

Samuel TC Brandt

Graduate Program in Biomedical Engineering

The Ohio State University

2020

Thesis Committee

Dr. Matthew A. Reilly, Advisor

Dr. Heather M. Powell, Committee Member

Dr. Mark Ruegsegger, Committee Member

Abstract

The molecular mechanisms driving age-related changes in lens material properties remains unknown. In this study, Raman spectroscopy was used to characterize structural differences in lens proteins between the cortex and nucleus, as well as changes resulting from exposure to acute ultraviolet (UV) radiation, a potential driver of age-related changes. Porcine lenses were obtained from a local abattoir and then used as control and experimental samples, separately. Nuclear and cortical lens protein portions were compared. Results were visualized, and statistical tests were performed to identify trends in protein structure. Protein concentrations in control samples matched published trends, while UV radiation produced changes in some lenses along with a cataract-like development in a single lens. While UV radiation changed capsular opacity in most samples, it caused opacification of the lens in one sample that coincided with other protein changes known to coincide with aging and cataract formation. Future studies should increase sample size and explore the dose-dependent changes in UV radiation exposure with both time and power adjusted to create different physiological simulations.

Dedication

To Katherine and all who believed in me.

Acknowledgments

I would like to thank my advisor for his direction and input and giving me the chance to undertake this research without guarantee.

Vita

June 2007.....Spanish Springs High School

December 2011.....B.A. English Writing and Philosophy, University of Nevada, Reno

May 2019.....B.S. Biomedical Engineering, The Ohio State University

June 2017 to present……Research Assistant, Department of Biomedical Engineering, The Ohio State University

August 2019 to present……Graduate Teaching Assistant, Department of Biomedical Engineering, The Ohio State University

Fields of Study

Major Field: Biomedical Engineering

Table of Contents

Abstract ii
Dedication iii
Acknowledgments iv
Vita v
List of Figures vii
Chapter 1: Introduction 1
Methodology Background 2
Lens Physiology 3
Raman Spectroscopy Theory 7
Raman Analysis Techniques 10
Statistical Methods 15
Chapter 2: Methods 16
Tissue Preparation 16
Raman Recording and Analysis 17
Lens Opacity 21
Chapter 3: Results 23
Program Verification 23
UV Treatment 26
Chapter 4: Discussion/Conclusions 41
Limitations 46
Future Work 48
Chapter 5: References 51

List of Figures

Figure 1: Anatomical diagram of the human adult lens. The cortex (‘C’) makes up the outer most layer. The nucleus (‘N’,aged form newest to oldest moving inward) makes up the bulk of the lens. 2
Figure 2: The fundamental principle of Raman scattering as exhibited on a tryptophan amino acid where there is a change in frequency and wavelength of scattered laser light [44]. The amount of change in the wavelength helps determine the structure of the scattering molecule. 9
Figure 3: Characteristic spectrum of typical porcine and human lens. The different peaks correspond to different detected levels of a given species or structure. These are based on comparisons within a library of spectra for different known particles. 10
Figure 4: Raman spectrum of the porcine lens in the 700-900cm-1 region. The tryptophan and tyrosine peaks are labeled, and the relative peak heights are compared within proteins as a measure of aging. 12
Figure 5: Raman spectrum of the porcine lens in the 1200-1700cm-1 region. The A1 and A3 peaks are labeled, and their composition can indicate relative abundance of α-helix and β-sheet secondary protein structures. 14
Figure 6: One method of spectral decomposition is peak deconvolution. The figure shows how the A1 region of the lens Raman spectrum can be deconvoluted into at least three distinct peaks. Each of these peaks has been shown to be associated with a particular protein type or conformation. 15
Figure 7: Raman spectrum of the porcine lens nucleus before and after correction with the ModPoly algorithm. Notice that after correction, the spectrum is flatter, which can be an issue in making peak comparisons. 18
Figure 8: Process flow diagram of Raman collection and analysis process. Raw data is background and baseline corrected prior to peak deconvolution analysis. (Zetasizer Helix image from [55]) 20
Figure 9: The areas of the expected β-sheet and α-helix peaks are calculated using ‘ipf’. In the above figure, the A1 region’s β-sheet (red) and α-helix (blue) peaks are highlighted. The ratio of the areas is recorded as well as the ratio of the areas. The A1 and A3 peak heights are standardized versus 1450cm^{-1} for numerical comparison. 19
Figure 10: (Left) Selection of a transparent lens area in the image processing function. The function compares the transparency of the lens radially versus the darkest portion of the control circle on the right (for both scale and darkness level). (Right) Output from the function showing transmission of visible light as a function of radius and the average as an integral over the area (transmission index). 22
Figure 11: Box plot of the tissue and wavelength intensity method in comparison. Each set of data represents a measure of β-sheet concentration relative to α-helix concentration. While deconvolution of the A1 and A3 bands of the nucleus and cortex yield highly variable answers, their values more closely align with prior measurements. The nucleus and cortex are statistically and visibly not different from each other despite the nucleus

and cortex known to be different in these respects. *Denotes statistical significance with a two-sample, two-tailed t-test (α = 0.05)..... 24
Figure 12: Box plot of the tissue and peak comparison method in comparison. Each set of data represents a measure of β-sheet concentration relative to α-helix concentration. While deconvolution of the A1 and A3 bands of the nucleus and cortex yield highly variable answers, they show trends that are more expected in lens proteins. The nucleus and cortex are statistically and visibly not different from each other despite the nucleus and cortex known to be different in these respects. *Denotes statistical significance with a two-sample, two-tailed t-test (α = 0.05)..... 25
Figure 13: Comparison of the fitting error for both nuclear and cortical tissue in fitting the A1 and A3 peaks. The error was very similar across both tissue types, indicating the fitting issues are not specific to a tissue, but more likely with the method. 26
Figure 14: Comparison of α-helix levels for the A1 peak in cortical and nuclear tissue. Left-tailed, equal variance, paired t-tests were conducted on the tissue within the treatments between tissues. Left-tailed, equal variance, two-sample t-tests were conducted on the samples between treatments. The tests show that, prior to treatment, the cortex is nearly significantly higher in α-helices than the nucleus pre- and post-treatment (p = 0.0547 and 0.0508 respectively) and the levels of α-helices is nearly significantly greater pre-treatment versus post-treatment (p =0.0836)..... 27
Figure 15: Comparison of α-helix levels for the A3 peak in cortical and nuclear tissue. Right-tailed, equal variance, paired t-tests were conducted on the tissue within the treatments between tissues. Right-tailed, equal variance, two-sample t-tests were conducted on the samples. The differences are not significant, and the averages are quite near each other. The only exception is the post-treatment nucleus, which has a relatively higher concentration, though not significantly so..... 28
Figure 16: Comparison of β-sheet levels for the A1 peak in cortical and nuclear tissue. Right-tailed, equal variance, paired t-tests were conducted on the samples within treatments between tissues. Right-tailed, equal variance, two-sample t-tests were conducted on the samples between treatments. The levels of the nucleus β-sheets both pre- and post-treatment were significantly higher than the cortex pre-treatment (p = 0.0345 and 0.0316, respectively). While the difference post-treatment is not significantly larger for either pre- or post-treatment levels in the nucleus versus the cortex (p = 0.0547 and 0.1661, respectively), the trends are consistent with other reports. 29
Figure 17: Comparison of β-sheet levels for the A3 peak in cortical and nuclear tissue. Right-tailed, equal variance, paired t-tests were conducted on the samples within treatments between tissues. Right-tailed, equal variance, two-sample t-tests were conducted on the samples between treatments. The differences are not significant, and it does not appear as if treatment has any effect on either tissue, although the cortex post-treatment has larger variance. 30
Figure 18: Comparison of the tryptophan ratio ($880cm^{-1}/760cm^{-1}$) for cortical tissue. The difference is not significant, the average slightly higher, but the deviations are very similar for post-treatment samples. However, the deviation is much larger in the post-treatment samples as well. 31

Figure 19: Comparison of the tryptophan ratio ($880cm^{-1}/760cm^{-1}$) for nuclear tissue. The difference is not significant, the average slightly higher, and the deviation slightly lower for post-treatment samples. While not statistically significantly different, the deviation for the pre-treatment samples was much larger. 32
Figure 20: Relative measured level of tryptophan content in lens protein tissue ($880cm^{-1}/760cm^{-1}$) pre- and post-UV treatment. There are no statistically significant differences between treatments or within tissues, although both the nucleus and cortex trended less post-UV treatment. 33
Figure 21: Comparison of the tyrosine ratio ($855cm^{-1}/830cm^{-1}$) for cortical tissue. The difference is not significant, the average slightly higher, but the deviations are much larger for post-treatment samples. 34
Figure 22: Comparison of the tyrosine ratio ($855\ cm^{-1}/830cm^{-1}$) for nuclear tissue. The difference is not significant, the average slightly higher, but the deviations are larger for post-treatment samples. 35
Figure 23: The average transmission for the lenses with capsule intact post-UV treatment were significantly lower according to a left-tailed t-test ($\alpha = 0.05$). However, this difference disappears when the capsule is removed, indicating the capsule may be undergoing opacification, as opposed to the lens itself. However, though not statistically significantly lower, the values for post-UV treatments lenses after capsule removal are lower on average. 36
Figure 24: Raman spectra of cortical samples where measurements of opacity were taken before and after treatment. The samples that "rebounded" in transparency with removal of the capsule are plotted against the sample that did not (inset). Along with not regaining transparency with capsule removal (indicating opacification of the lens and not just the capsule), this sample also showed differences at many places in the spectrum, including in the tryptophan and tyrosine ratios as well as peak shifts in the A1 and A3 peaks. Another notable change is in the $500\text{-}600cm^{-1}$ region, which is associated with changes in sulfide bonding. Peaks around $500cm^{-1}$ indicate the presence of oxidized sulfide bonds, leading to disulfide bonds not originally present or between otherwise not typically bonded sulfurs. 38
Figure 25: Close up on the disulfide, tyrosine, and tryptophan areas of interest of the cortical samples mentioned in Figure 22. The samples that "rebounded" in transparency with removal of the capsule are plotted against the sample that did not (inset). Along with a change in the tyrosine ratio ($855\ cm^{-1}/830cm^{-1}$), the figure calls out the tryptophan peak that may be linked to an exposed and oxidized tryptophan amino acid. Also labeled on the figure is the presence of peaks at $500\ cm^{-1}$ and $545\ cm^{-1}$. These peaks are indicative of sulfurs present that were oxidized and formed disulfide bonds. While disulfide bonds are present in lens proteins, other paper studies have shown that peaks of this nature indicate misfolding due to bonds between sulfurs that are not bound together in healthy, young lens tissue. 39
Figure 26: Raman spectra of cortical samples where measurements of opacity were taken before and after treatment. The samples that "rebounded" in transparency with removal of the capsule are plotted against the sample that did not (inset). Although the cortical sample showed difference in its spectrum (see Figure 22), the nucleus appears mostly

unchanged among the samples. This may indicate that the changes incurred did not reach “as deep” as the nucleus, or that the nucleus is otherwise protected by changes of that magnitude..... 40

Chapter 1: Introduction

Presbyopia is the progressive, age-related loss of the eye's ability to focus on nearby objects. Age-related cataract is the progressive opacification of the lens. Presbyopia presents clinically in middle age, whereas age-related cataract generally presents in advanced age. While presbyopia presents clinically in nearly 100% of patients, and cataract is the leading cause of blindness worldwide, their molecular operative mechanisms are poorly understood.

Inhibiting our understanding of these molecular mechanisms is the lack of a suitable long-lived animal model for age-related changes, high variability of environmental insults in human donor lenses, and the lack of suitable *in vitro* models. In this study, we sought to investigate the suitability of the porcine model as an *in vitro* model for aging and cataract formation. This requires the use of young pig lenses which have been shown to have low inter-sample variability, and are biochemically and biomechanically similar to young human lenses.

The goal of the presented study is two-fold: first, develop and verify a program meant to automatically analyze lens tissue via Raman spectroscopy; second, study the changes to lens tissue with a common pathological insult associated with aging and cataract formation. Young porcine lenses were exposed to ultraviolet (UV) radiation in an effort to simulate aging and cataract formation. Specifically, this study focuses on the differences in response to UV radiation by the lens cortex and nucleus measured both by Raman spectroscopy and lens opacity. Figure 1 is a diagram of the composition of an

adult lens by cortex and nucleus [1]. The lens cortex and nucleus respond differently in aging and cataract formation [2].

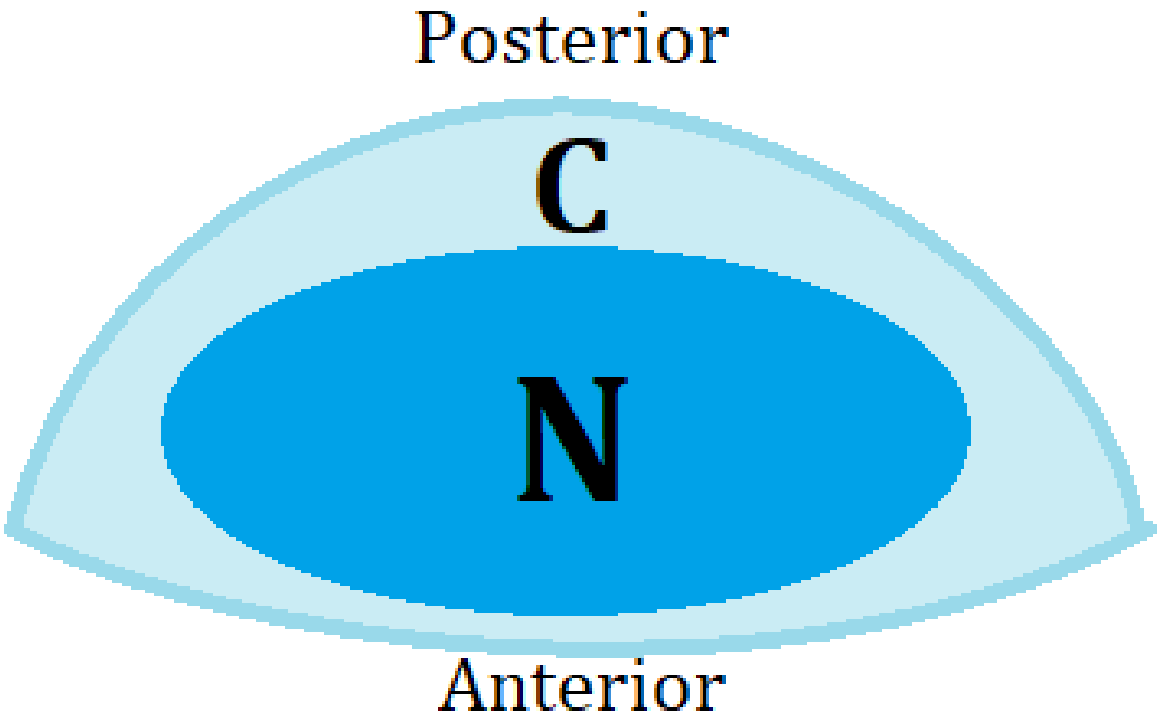

Figure 1: Anatomical diagram of the human adult lens. The cortex (‘C’) makes up the outer most layer. The nucleus (‘N’, aged form newest to oldest moving inward) makes up the bulk of the lens.

Methodology Background

The nucleus is the oldest part of the lens and begins formation before birth [1]. While the exact definition of the nucleus and cortex varies, in this paper, the nucleus can be considered the denser, inner portion of the lens, while the cortex is the newer, softer portion. This means that while both the nucleus and cortex are susceptible to post-

translational modifications, the cortex is much more likely to be modified by environmental insults that lead to pathological modifications.

Age-related nuclear (ARN) cataract is the most common form of cataract [3]. A number of theories have been proposed to explain the mechanisms of ARN cataract formation, but risk factors include alcohol consumption, diabetes, and UV exposure. Research about cataracts and ARN cataracts have centered on different aspects of protein change, and Raman has been used to investigate these changes in various aspects of the lens. Investigations include the Amide I (A1) and Amide III (A3) bands (reflections of α-helix and β-sheet content), tryptophan and tyrosine residues, disulfide bonding, and other lens protein and lipid components and structures [4].

Raman spectroscopy was first theorized and investigated in the early 20th century by C.V. Raman [5]. Many investigations attempted to understand how different structural changes reflected in the Raman spectrum, and shortly after, Amide modes were attributed to certain bending or stretching modes [6]. From these groupings, it was deduced what structures would be inherent within each modality. This includes the contributions of secondary structures to various modes. The lens protein spectrum contains two dominant amide modes: A1 and A3 [7]. These two modes, characterized by C=O stretch and C-N stretch and N-H bend (respectively), can help determine the relative amounts of ordered secondary structures, as well as other disordered and hydrogen-bonded structure [5].

Lens Physiology

Both the nucleus and cortex undergo protein modifications with age. The differences between cortical and nuclear lens tissue with age have not fully explored;

however, it is generally seen that there are increased levels of β-sheet content in the nucleus, and the amount of β-sheet content may increase with cortical cataract formation [8]. On the other hand, the level of α-helix content increases with noncortical cataract formation according to the same study. Other studies have found no correlation [9]. One study found that changes in A1 protein distribution that occurred with lens yellowing and where changes in tryptophan and tyrosine occurred, but the changes in α-helix and β-sheet content were not necessarily concomitant [10]. These changes were found to occur with changes in other structures and lipid changes though.

Tryptophan may act as a filter for UV light, but also can be detected as bound to other proteins after oxidation [11]. The literature is controversial for tryptophan evolution with cataract formation, with some studies showing a decrease in certain Raman intensities with cataract formation [12] [9], while others have shown increase in actual tryptophan levels with cataract formation in humans [13]. Aging results in animal models have been mixed [14]. These discrepancies could be due to the difference between bound tryptophan and other forms of it, which may change over time and between animal models. Many studies have shown that the intensity peak at 880cm^{-1} can detect the exposure level of the tryptophan, with a higher intensity indicating a “buried” tryptophan that is not hydrogen bonded [15]. For that reason, aged and opaque lenses are expected to show an exposed, hydrogen bonded tryptophan that has a low intensity at 880cm^{-1}.

Tyrosine may also act as a catalyst for UV filters and is elevated in human cataractous lenses [13]. Changes in tyrosine may be related to changes in hydrophobicity and water content, while also being an indicator of cortical cataracts [16] [12]. One study

showed a change in the tyrosine doublet at 855/830cm^{-1} with cold cataracts, which may indicate the tyrosine microenvironment in developing light scattering effects [17]. These types of changes were also observed in lens opacification with aging in mouse lenses [18]. In humans, tyrosine may be unevenly hydrogen bonded, which may be linked to the opacification [19].

One theory of protein misfolding leading to lack of accommodation ability and cataract is the change of disulfide bonding in the lens [20] [3]. Disulfide bonding is a suspected mechanism of either being causative or correlative with lens cataracts and aging [7] [21] [22] [23]. Intramolecular disulfide bonds exist in the healthy state of the lens for humans and many other animals. These bonds may readily oxidize and reduce in a healthy environment to preserve the structure of the lens [21]. While this mechanism is important in maintaining lens health, “runaway” disulfide bonding may lead to intermolecular “kinks” that cause aggregation within the lens, leading to both lens stiffening and potentially cataract-level opacification [22]. However, not all cataracts may stem from disulfide misbonding and accompanying protein misfolding. Other studies have shown “healthy” or “normal” disulfide bonding in human aged and cataract lenses [8] [24].

There are three categories of crystallin proteins in the human lens fiber cells: α, β, and γ [25] [26]. These different crystallin proteins make up 90% of the protein in the human lens [27]. Each of these classes of protein have subtypes that have different functions, and are common to the lenses of many animals, including pigs and cows [28] [29] . Other species, like certain avian species, have δ-crystallin proteins not present in

humans and other animals [30]. In short, all act as structural proteins, while α class proteins also act as chaperones against protein denaturation [25] [31].

α crystallin proteins are multimeric and the largest of the protein classes. They provide protection against denaturation similar to heat shock proteins (hsps) [32] and a loss of functional, unmodified α crystallin proteins is correlational with age and other aging effects [31]. Hsps exist in many forms and were first discovered in relation to denaturation related to heat (thus the name) [33]. Despite the name, hsps have been shown to help prevent many types of protein degradation, and in the lens proteins, specifically oxidation. These unmodified proteins also tend to decrease in abundance with age, and are found in lower abundances in human patients with ARN cataracts [34]. One study showed that upon various post-translational modifications (PTMs), the presence of α crystallin proteins in the nucleus is reduced and aggregates of other proteins is increased [35]. This may indicate better protection of lens proteins in the cortical region.

β and γ crystallin proteins are smaller than α crystallin proteins, and are sometimes within the same crystallin superfamily [36]. While β crystallin proteins may join multimeric protein units, γ crystallin proteins are monomeric and the smallest of all crystallin proteins. In particular, γ proteins are much higher in density in vertebrate animals and may contribute to packing density, clarity, and lens (in)flexibility.

The protein in the lens fibers consist mostly of β-sheets with some α-helices and other random coil and turn structures present [37] [38]. Different crystallin classes have different distributions of secondary protein structures, but in general, the two important

secondary structures (α-helices and β-sheets) are on average 1:1 across lens tissue [8] [39].

In addition to proteins being classified by class, proteins can also be separated on the basis of solubility (or non-aggregation) [40]. Water soluble (WS) lens content consists mostly of whole, unmodified proteins, while water insoluble (WI) lens content consists of fragments or truncations of various proteins along with fats and cholesterols. The amount of truncation and cleavage may be tied to age and cataract presence. Specifically, human cataractous lenses may contain WI proteins that are truncated, have oxidized tryptophan proteins, and asparagine deamidated to aspartic acid.

Another area of study is water content. In general, the amount of bulk, unbound water in the lens increases with age, and the lens has variations along the equatorial region, but less so in the anterior and posterior poles [41]. The water content in the cortical equator is also generally higher than the posterior or anterior cortical regions [42]. While not all opaque spots in the first study were correlated with water changes, there were cortical opacities that were correlated with bulk water in some samples [41]. In general, the nucleus contains less water, bound and bulk, than the cortex. Though water content can be studied using Raman techniques, the current study does not include it as the capacity of the equipment used does not allow the required higher frequencies.

Raman Spectroscopy Theory

Raman spectroscopy is a method of measuring protein presence and relative abundance by wavelength changes in coherent infrared spectra. Equation 1 demonstrates the calculation for Raman shift, which is ultimately how proteins and bonds are measured

using Raman intensity data [43]. The intensity data are captured at different wavelengths (and therefore frequencies).

$$\omega = \overline{\nu_m} - \overline{\nu_0} = \frac{\nu_m - \nu_0}{c} \quad [1]$$

Equation 1: Calculation of the Raman Shift (ω). $\overline{\nu_m}$ is average measured frequency, while $\overline{\nu_0}$ is the excitation frequency, and c is the speed of light in a vacuum.

Other factors may affect Raman shift, as the frequency is not a simple measurement but is affected by electromagnetic fields, dipole moments, and other factors. However, Equation 1 is the foundation of the calculation.

Figure 2 is an illustration of how frequency change occurs as a result of wavelength (λ) change. The Raman scattering is inelastic scattering that results in an increased frequency. This is the frequency along with the source frequency used in Equation 1 to calculate Raman shift.

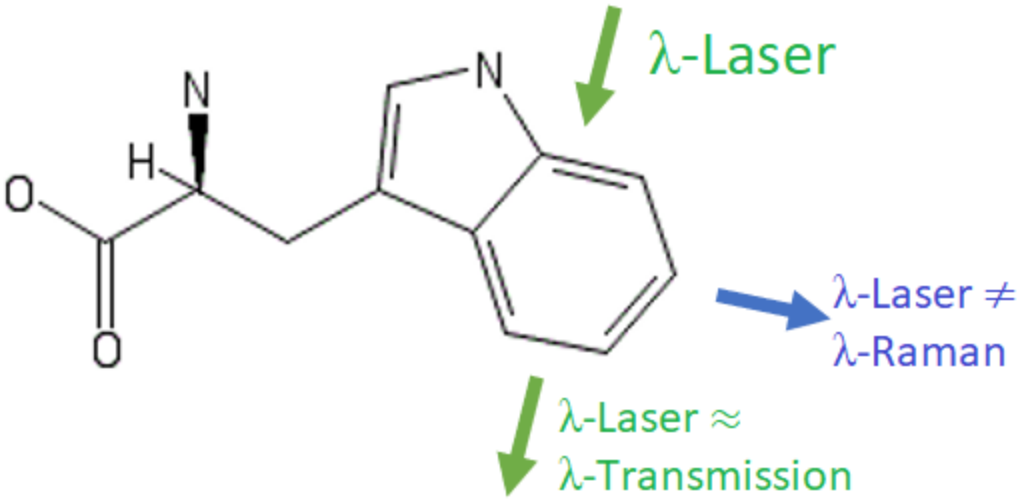

Figure 2: The fundamental principle of Raman scattering as exhibited on a tryptophan amino acid where there is a change in frequency and wavelength of scattered laser light [44]. The amount of change in the wavelength helps determine the structure of the scattering molecule.

The lens Raman spectrum has been well characterized [4]. Figure 3 is a characteristic spectrum with known peaks labeled. This zone, from ~400cm^{-1} to ~1750cm^{-1} is known as the "fingerprint" area of the spectrum and is most unique to the lens. While the fingerprint area of the spectrum can reveal the most about protein configuration, water content and protein oxidation can also be described in the region "above" 1800cm^{-1} [42] [24]. Disulfide bonds, for example, may be reflected in both areas, with changes near 508cm^{-1} and 2580cm^{-1} happening with changes in disulfide bonding and water content.

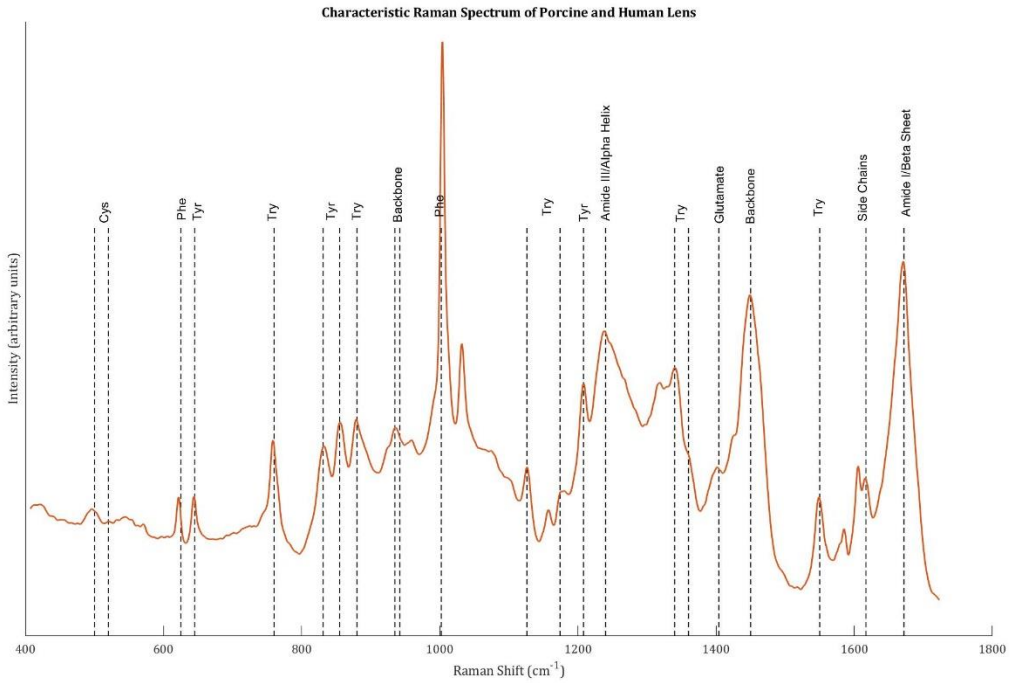

Figure 3: Characteristic spectrum of typical porcine and human lens. The different peaks correspond to different detected levels of a given species or structure. These are based on comparisons within a library of spectra for different known particles.

Raman Analysis Techniques

Methods have been developed to measure protein composition in Raman spectra [45] [46]. Techniques for determining relative concentration range from peak height comparison to spectral decomposition. Though methods utilizing peak height are simpler and can be used in some cases, spectral decomposition or peak fitting is required to unravel more complex formations.

Peak height comparison can be used for measuring relative tryptophan and tyrosine changes [45]. In either case, a measured peak is compared to a reference peak. In

the case of tryptophan, the reference peak is a backbone peak that theoretically does not change due to stress or other factors [47]. Tyrosine, on the other hand, is compared with a separate tyrosine peak, and the relative levels are correlated with microenvironmental changes that occur in cataract formation.

Intensity comparison at specific wavenumber is another technique utilized in Raman spectroscopic analysis [4]. This technique simply measures the relative intensity of a specific wavenumber versus a control peak (typically the protein backbone or a stable amino acid residue) [8]. This technique was compared to the technique developed in this study to compare physiological relevance of either technique when compared to known literature values.

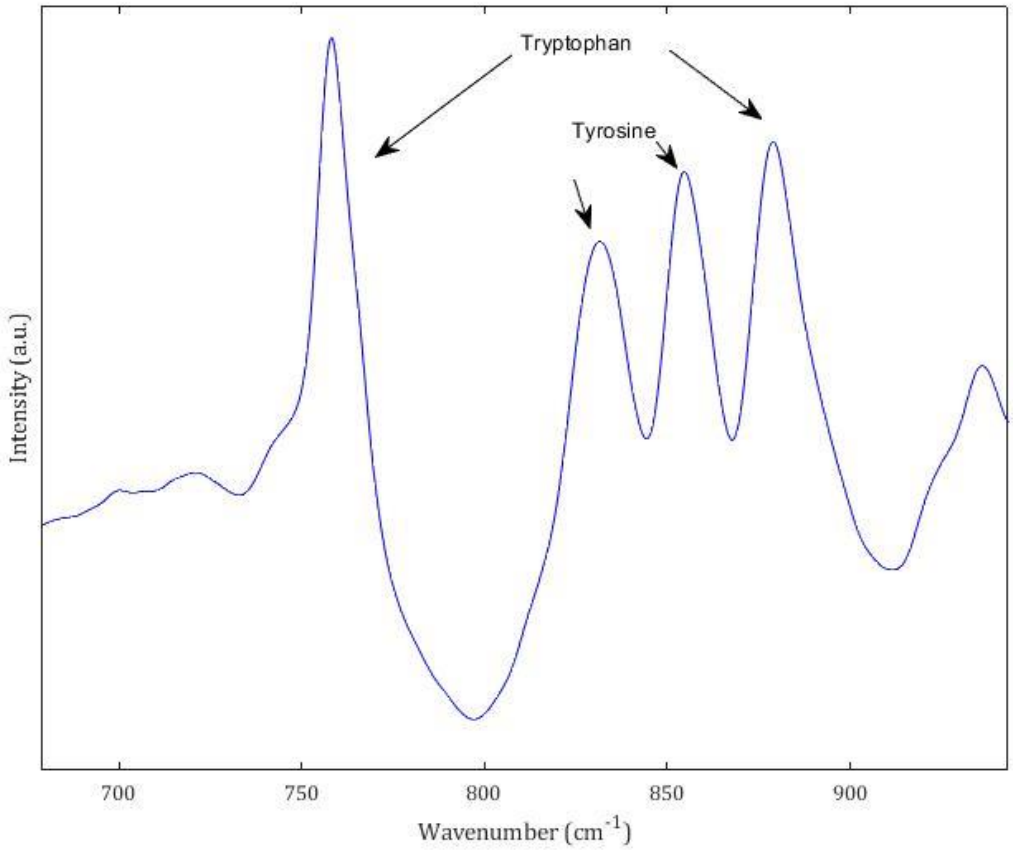

Figure 4: Raman spectrum of the porcine lens in the 700-900cm^{-1} region. The tryptophan and tyrosine peaks are labeled, and the relative peak heights are compared within proteins as a measure of aging.

Spectral decomposition is the process of determining components of Raman spectra by various fitting methods [46]. The basic idea is that if a peak is known to be composed of different protein types or formations, then a fitting model can decompose a peak into its components. This particular technique has been used in Fourier transform infrared spectroscopy as well as other signal analysis modes [48]. This technique is also

sometimes known as characteristic fitting as the fitting parameters are based on peaks that are exemplary of the protein, structure, or formation in question [49].

A lingering question with Raman spectroscopic analysis is physiological relevance. Though techniques exist that can break spectra down into mathematically well-fit peaks, this doesn't necessarily mean that these peaks provide relevant physiological information [50]. There is a question of interpretation in these techniques as the peaks are not necessarily representative of known protein peaks. While Raman spectroscopy can differentiate spectra to a higher accuracy, it has its own limitations in time and fluorescent interference [51] [52]. Therefore, techniques that can parse biological data that is physiologically relevant is important to avoid mistaking noise for data.

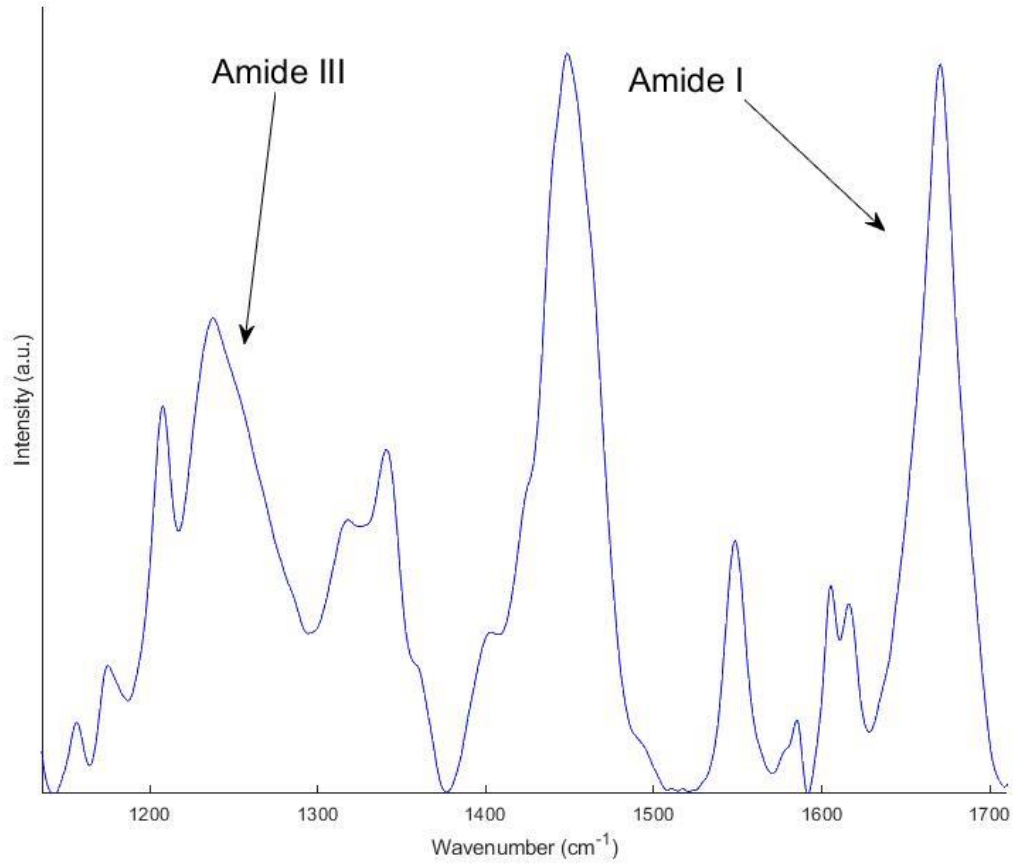

Figure 5: Raman spectrum of the porcine lens in the 1200-1700cm^{-1} region. The A1 and A3 peaks are labeled, and their composition can indicate relative abundance of α-helix and β-sheet secondary protein structures.

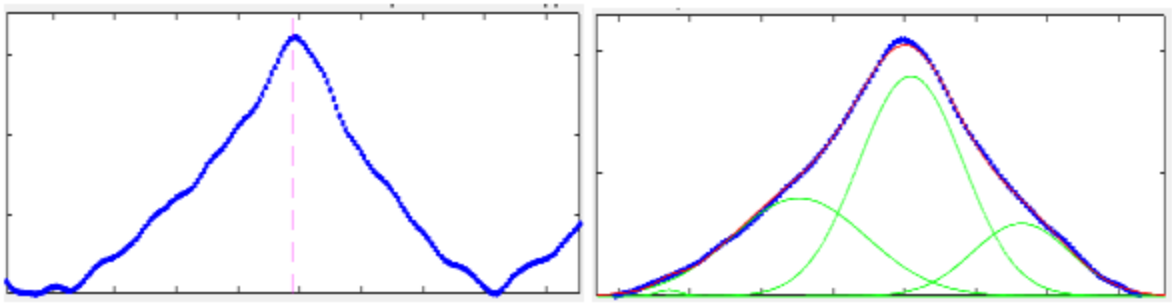

Figure 6: One method of spectral decomposition is peak deconvolution. The figure shows how the A1 region of the lens Raman spectrum can be deconvoluted into at least three distinct peaks. Each of these peaks has been shown to be associated with a particular protein type or conformation.

Many programs exist for this process. 'ipf' is an interactive peak fitting program that can be used to deconvolute a signal using multiple peak shapes [53]. This program can be utilized with the proper settings to decompose the A1 and A3 peaks. In both cases, error will be reduced as much as possible to ensure the best fit. Settings will vary based on which peak is being analyzed due to differences in spectral composition. The author composed a program in MATLAB to automatically fit the A1 and A3 peaks, as well as report peak comparison data on the tryptophan and tyrosine peaks.

Statistical Methods

To determine if UV radiation causes a statistically significant change in the levels measured (β-Sheet and α-Helix for A1 and A3, Tryptophan, and Tyrosine), an appropriately tailed, equal-variance t-test will be used.

Chapter 2: Methods

Tissue Preparation

Young porcine lenses were obtained from a local abattoir. Each lens was dissected with the capsule intact. The intact capsular lenses were then transferred to a M-199 solution with added glutamine and antibiotics (as preservatives). The lenses were then placed in a 37°C lab air incubator. After 16-20 hours of incubation, the lenses were examined to determine if the epithelial cells were alive (an indication of a healthy lens). Healthy epithelial cells are invisible, whereas dead cells cause opacities in the lens. The lens was then visually inspected for opacification and, if still transparent, was used for Raman testing.

In order to separate the lens nucleus and cortex, the capsule was removed with forceps and discarded and the lens was pulled apart along the lens sutures [54]. In short, this consisted of carefully opening the lens with forceps and pulling the sutures apart. Then, the lens nucleus was extracted from the center of the opened lens.

The nucleus and cortex were further sectioned by using a 3.5mm biopsy punch. For consistency, the center portion of the nucleus and anterior-center portion of the cortex were both punched and separated for analysis. The tissue samples were placed in a titanium microcuvette with 125μm-thick quartz windows [55]. The remaining volume in the cuvettes was filled with PBS solution.

Raman Recording and Analysis

Raman intensity data were recorded five times each for each sample and portion. Each record was composed of two scans at 20 seconds per scan. The Raman excitation laser frequency was 785nm.

Background correction was completed using proprietary Malvern software [56]. Baseline correction of the spectra using ModPoly was also completed prior to analysis [57]. This program essentially corrects the baseline by fitting a polynomial to the spectrum and subtracting it to make the baseline flat. Figure 7 shows how ModPoly can "correct" a spectrum prior to analysis.

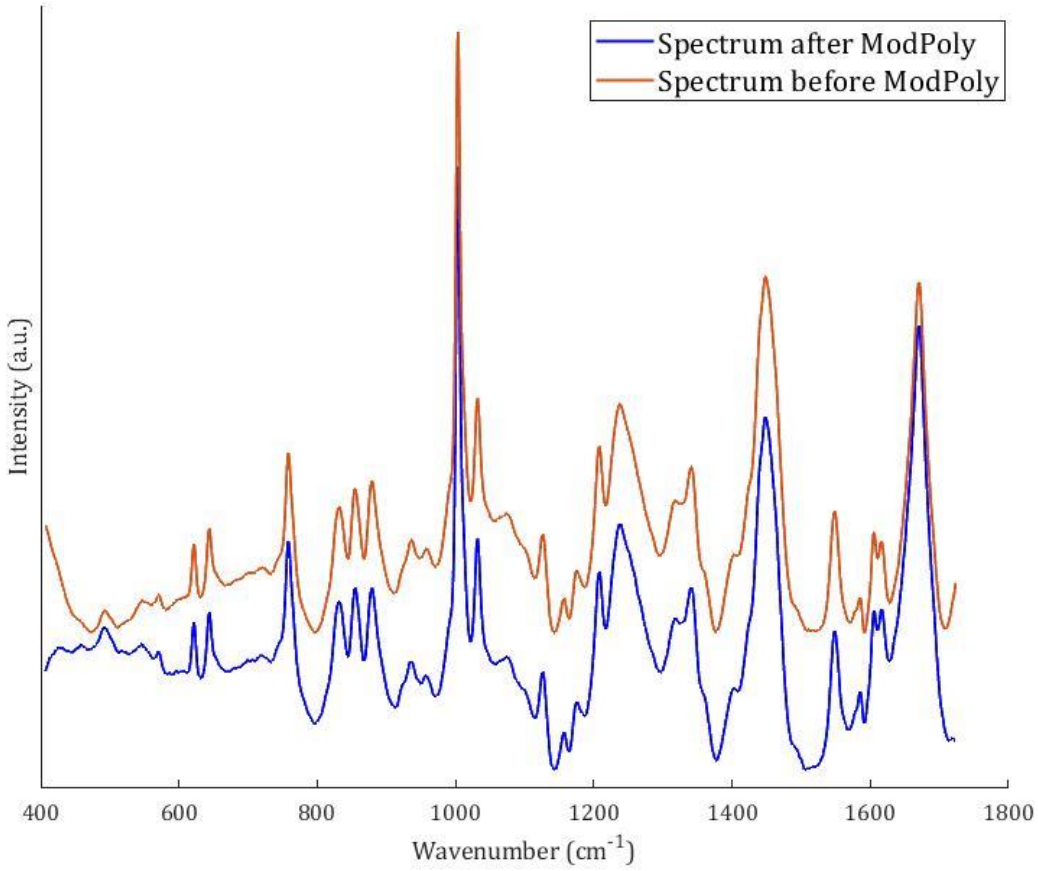

Figure 7: Raman spectrum of the porcine lens nucleus before and after correction with the ModPoly algorithm. Notice that after correction, the spectrum is flatter, which can be an issue in making peak comparisons.

Raman peak areas were compared according to other experiments to determine sulfide bonding, protein evolution, and secondary structure changes [14] [24] [7] [8]. All peak analysis was completed in MATLAB2020R1 [57].

For the A1 and A3 secondary protein abundances, 'ipf' was run with a scanning setup for each of four possible peak assignments and widths. In each region, the relative abundance of β-sheets was calculated as the area of the expected area for β-sheets versus

the expected area for α-helices as well as the area normalized to the 1450cm^{-1} peak.

Figure 8 demonstrates the peak areas for the A1 region and what is compared. Figure 9 is a process map of the analysis process.

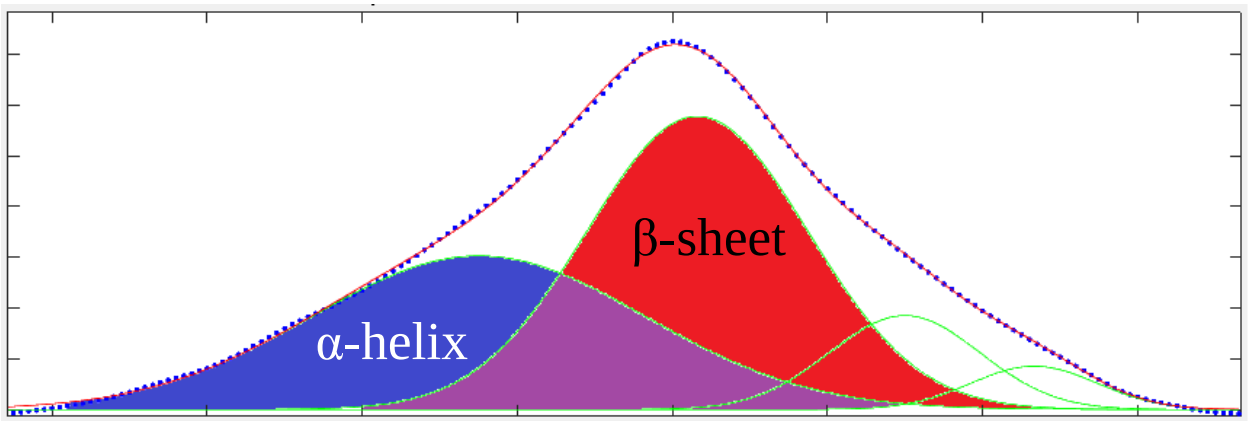

Figure 8: The areas of the expected β-sheet and α-helix peaks are calculated using 'ipf'. In the above figure, the A1 region's β-sheet (red) and α-helix (blue) peaks are highlighted. The ratio of the areas is recorded as well as the ratio of the areas. The A1 and A3 peak heights are standardized versus 1450cm^{-1} for numerical comparison.

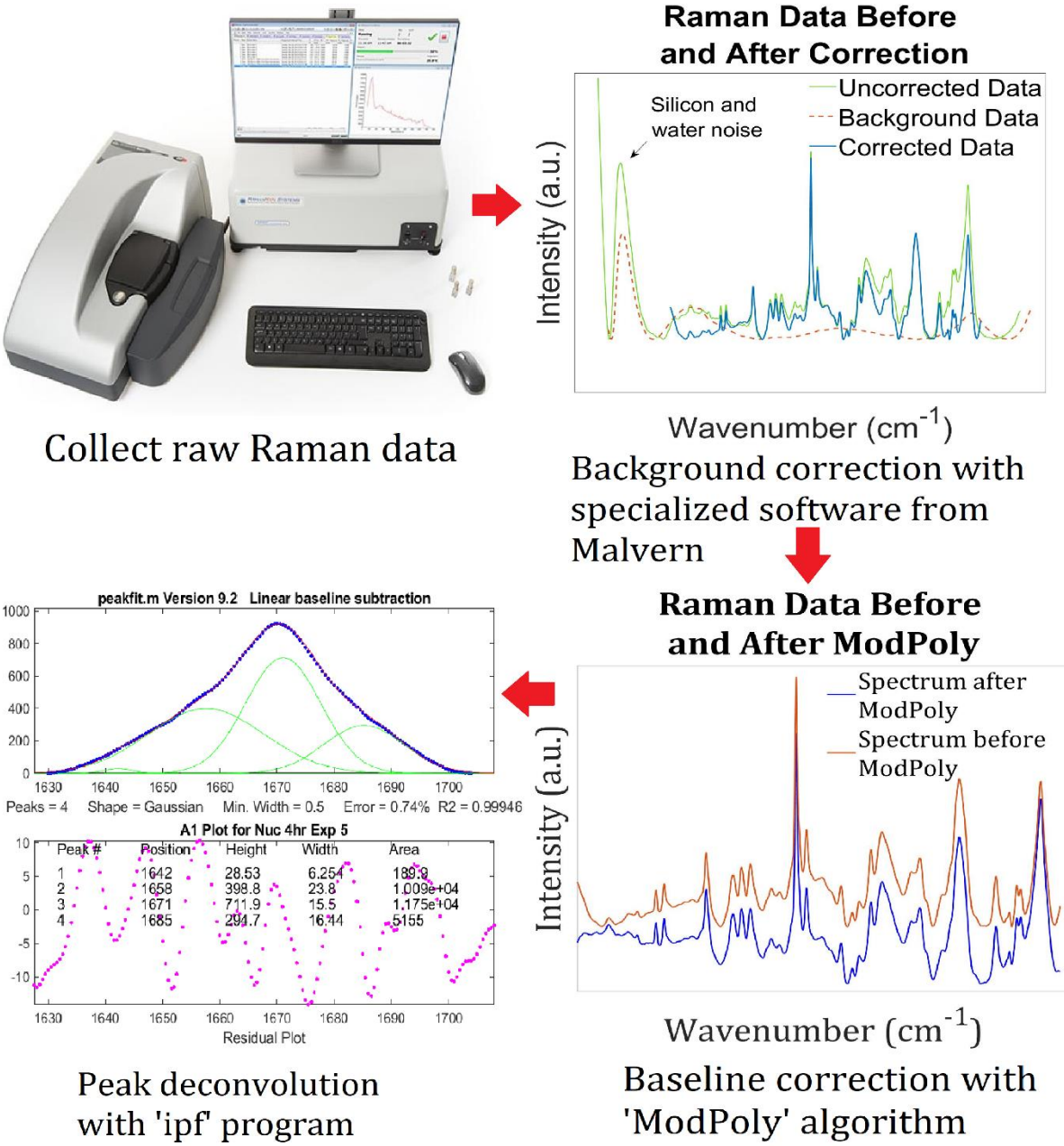

Figure 9: Process flow diagram of Raman collection and analysis process. Raw data is background and baseline corrected prior to peak deconvolution analysis. (Zetasizer Helix image from [55])

For the tryptophan and tyrosine peak height comparison, peaks were compared using a MATLAB function composed by the author. It was a simple measured height of the two peaks for each protein, and the output was a ratio of these values. Relative exposure and the microenvironment of tryptophan was made by comparing the peak heights of $880cm^{-1}/760cm^{-1}$, while relative tryptophan content was assessed by comparing the peak heights of $760cm^{-1}/1450cm^{-1}$. The tyrosine microenvironment was characterized by comparing the peak heights of $855cm^{-1}/830cm^{-1}$.

Lens Opacity

Lens opacity was measured using a program designed by the authors that measures the average intensity under the curve for the white color in an RGB format. Images of the lenses either pre-treatment, post-treatment, or post-treatment without the capsule were taken for each sample. These averages were compared across groups, and individual lenses were analyzed with regard to their individual results in other areas.

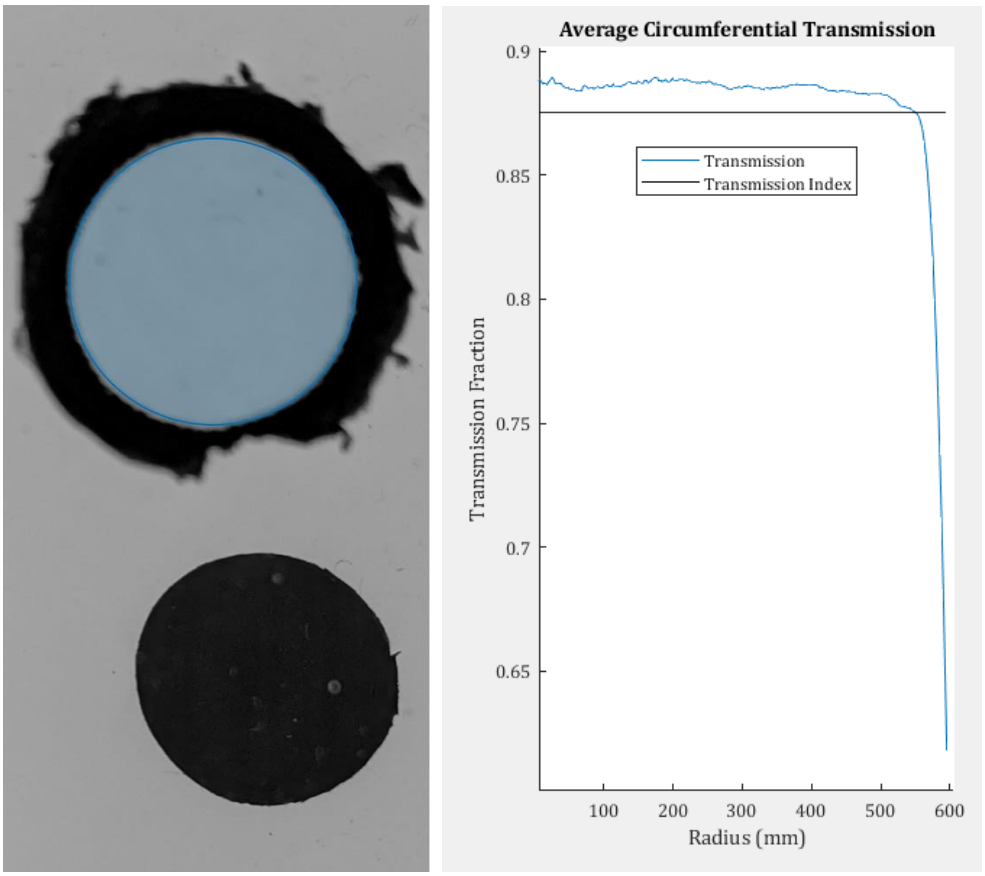

Figure 10: (Left) Selection of a transparent lens area in the image processing function. The function compares the transparency of the lens radially versus the darkest portion of the control circle on the right (for both scale and darkness level). (Right) Output from the function showing transmission of visible light as a function of radius and the average as an integral over the area (transmission index).

Chapter 3: Results

For the A1 and A3 peaks within a treatment between samples, the samples are paired with n = 5. For the A1 and A3 peaks, tryptophan, and tyrosine comparisons, the samples are not paired between treatment with n = 5.

Program Verification

To verify the analysis algorithm, comparisons were made between secondary protein structures in the nucleus and cortex. Figure 11 and Figure 12 are box plot comparisons of tissue and technique analyses. Two-sample, two-tailed, equal variance t-tests ($\alpha = 0.05$) were utilized to determine if there are differences between or within the methods.

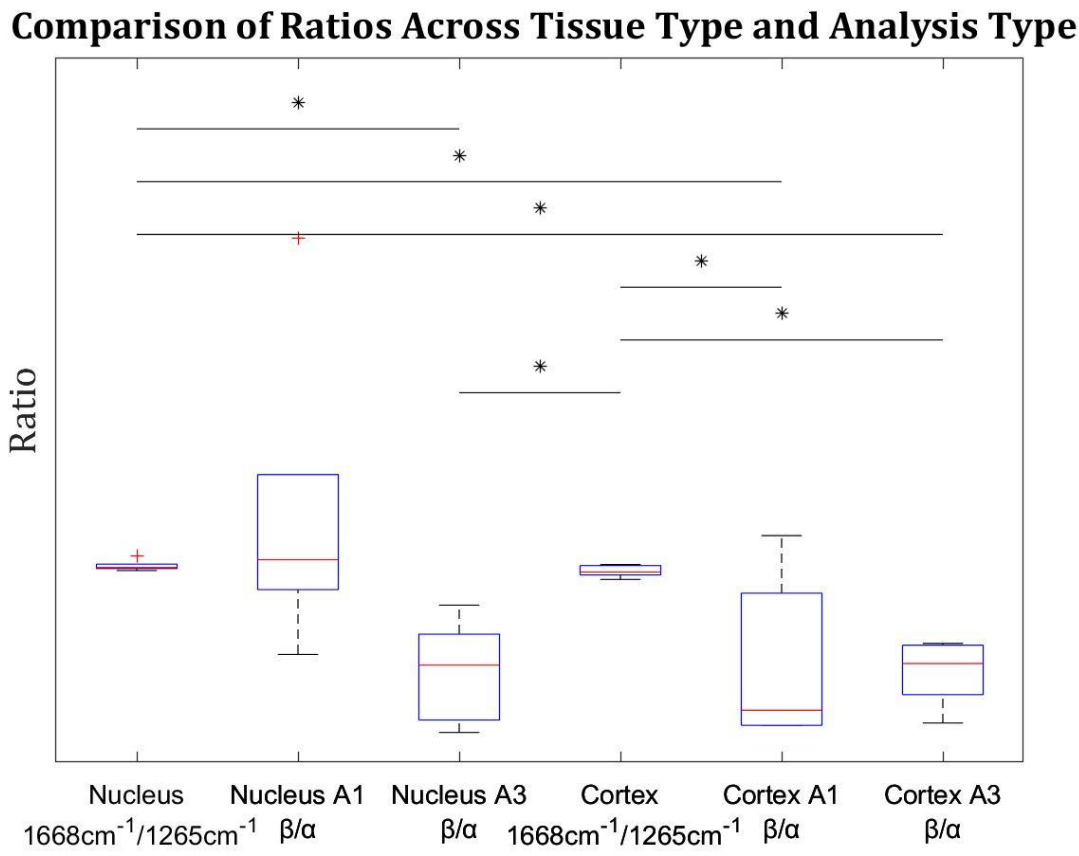

Figure 11: Box plot of the tissue and wavelength intensity method in comparison. Each set of data represents a measure of β-sheet concentration relative to α-helix concentration. While deconvolution of the A1 and A3 bands of the nucleus and cortex yield highly variable answers, their values more closely align with prior measurements. The nucleus and cortex are statistically and visibly not different from each other despite the nucleus and cortex known to be different in these respects. *Denotes statistical significance with a two-sample, two-tailed t-test (α = 0.05).

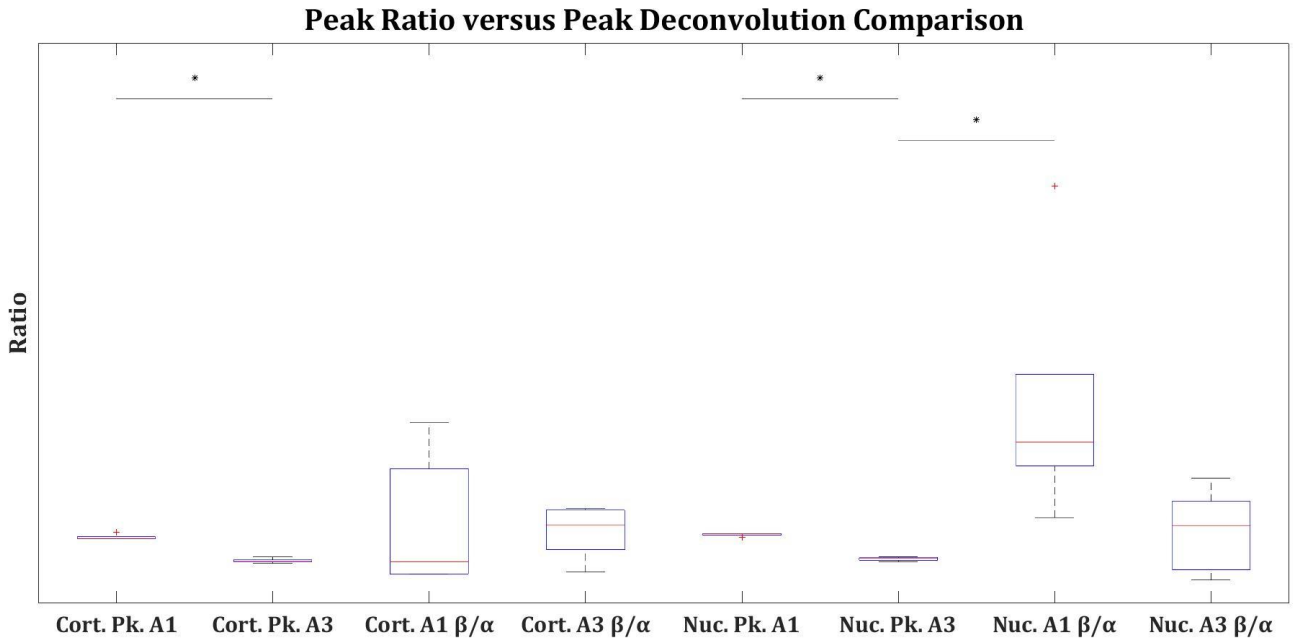

Figure 12: Box plot of the tissue and peak comparison method in comparison. Each set of data represents a measure of β-sheet concentration relative to α-helix concentration. While deconvolution of the A1 and A3 bands of the nucleus and cortex yield highly variable answers, they show trends that are more expected in lens proteins. The nucleus and cortex are statistically and visibly not different from each other despite the nucleus and cortex known to be different in these respects. *Denotes statistical significance with a two-sample, two-tailed t-test ($\alpha = 0.05$).

As this fitting method is novel, a comparison of fitting error across tissues and peaks illustrate that the A3 peak is a more error-prone peak to fit and neither tissue is more difficult than the other to obtain results. The nuclear tissue is more well fitted for A1, which may indicate the nucleus is protected from UV oxidation and aging by the cortex.

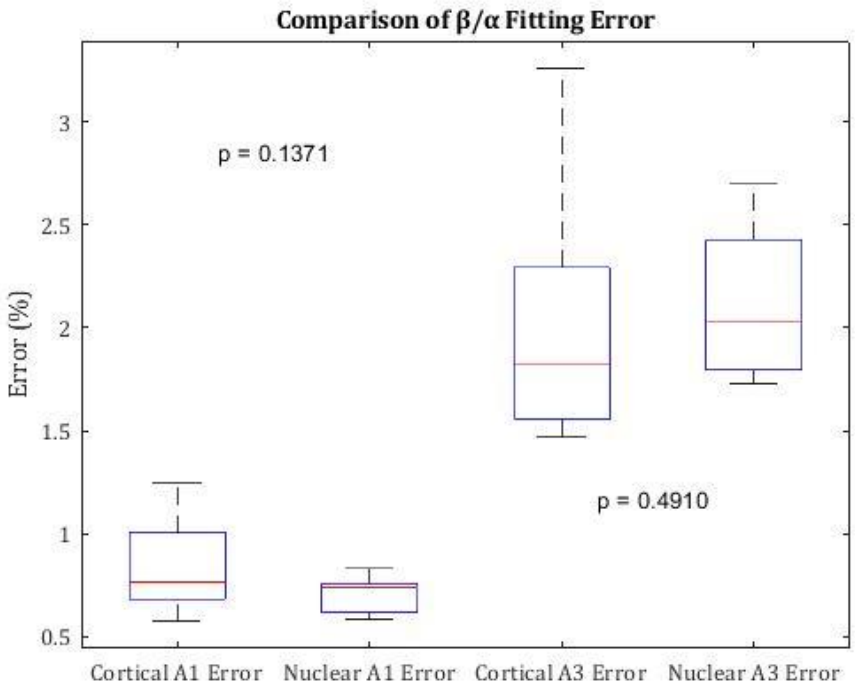

Figure 13: Comparison of the fitting error for both nuclear and cortical tissue in fitting the A1 and A3 peaks. The error was very similar across both tissue types, indicating the fitting issues are not specific to a tissue, but more likely with the method.

UV Treatment

Once validated, this software was used to estimate the alpha helix content of samples from the cortex and nucleus. According to Figure 14 and

Figure 15, the relative level of α-helices in the nucleus and cortex, as measured in the A1 and A3 peaks, is not significantly different between tissues or between treatments. However, it appears that treatment, according to the A1 levels, reduces the concentration

of α-helices in the cortex. This may be important considering results in the A1 peak for β-sheets, as shown in Figure 16.

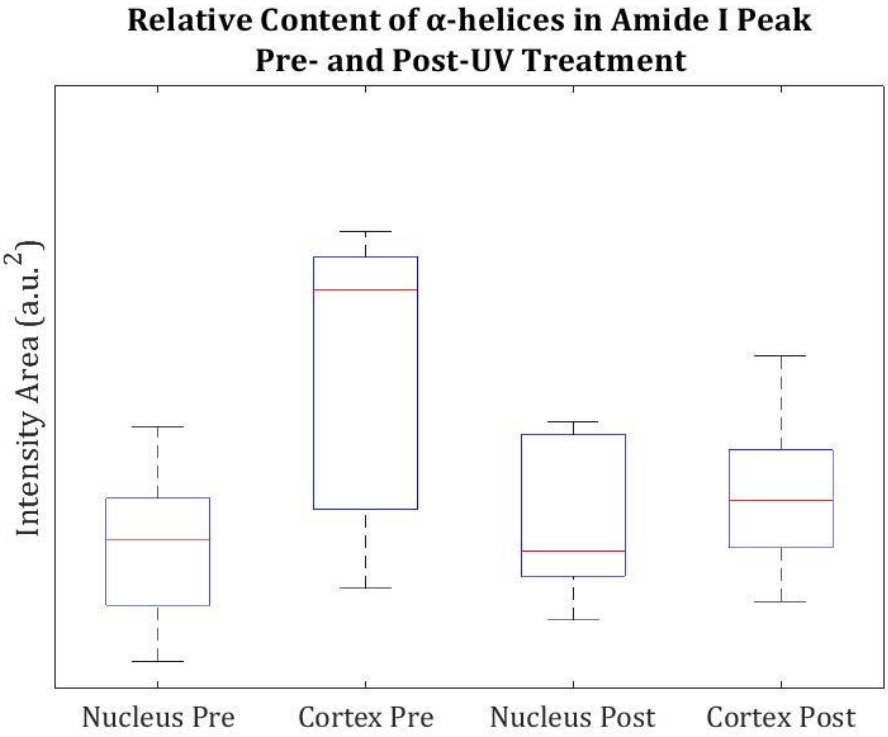

Figure 14: Comparison of α-helix levels for the A1 peak in cortical and nuclear tissue. Left-tailed, equal variance, paired t-tests were conducted on the tissue within the treatments between tissues. Left-tailed, equal variance, two-sample t-tests were conducted on the samples between treatments. The tests show that, prior to treatment, the cortex is nearly significantly higher in α-helices than the nucleus pre- and post-treatment ($p = 0.0547$ and 0.0508 respectively) and the levels of α-helices is nearly significantly greater pre-treatment versus post-treatment ($p = 0.0836$).

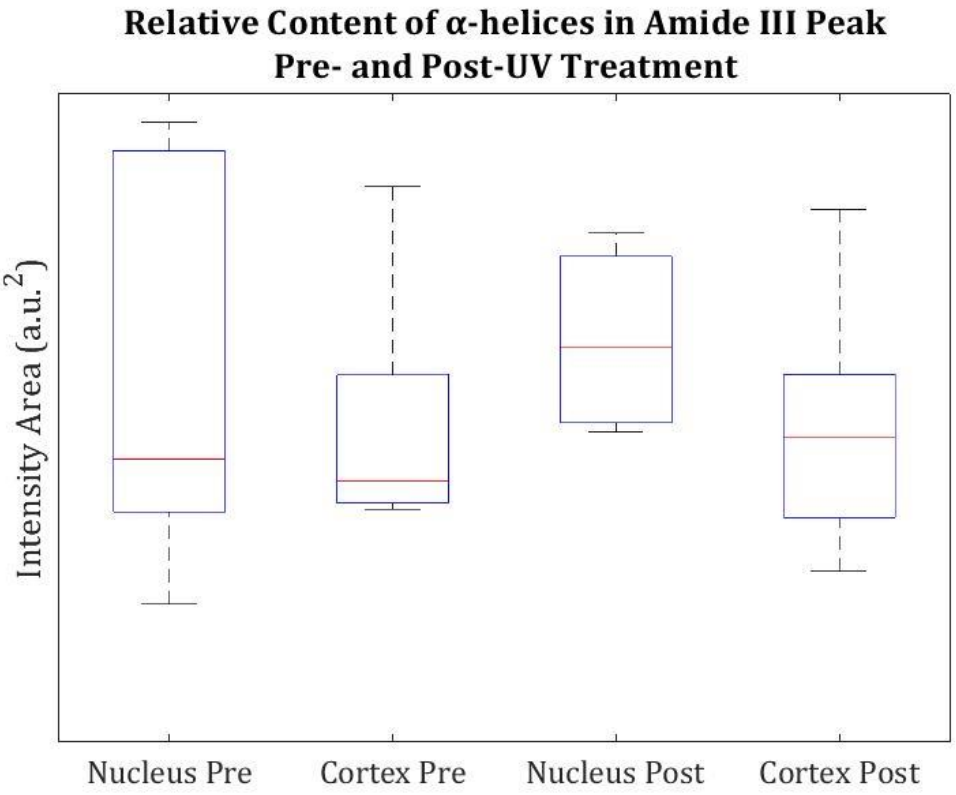

Figure 15: Comparison of α-helix levels for the A3 peak in cortical and nuclear tissue. Right-tailed, equal variance, paired t-tests were conducted on the tissue within the treatments between tissues. Right-tailed, equal variance, two-sample t-tests were conducted on the samples. The differences are not significant, and the averages are quite near each other. The only exception is the post-treatment nucleus (n = 5), which has a relatively higher concentration, though this difference did not rise to the level of statistical significance.

Figure 16 shows that the level of β-sheets is significantly higher in the nucleus versus the pre-treatment cortex both pre- and post-treatment. While the difference is not significantly higher in the nucleus versus post-treatment cortex, the trend remains the same and may be partially explained by the relative increase in α-helix content in the A1 peak post-treatment in the cortex.

Figure 17 is similar to

Figure 15 in that the A3 peak analysis shows relatively little difference in either tissue pre- and post-treatment. This may indicate that the A3 band is poorly fit, not susceptible to changes, or that the bending and stretching mode measured in the A3 peak is not affected by UV treatment and not different within the tissues.

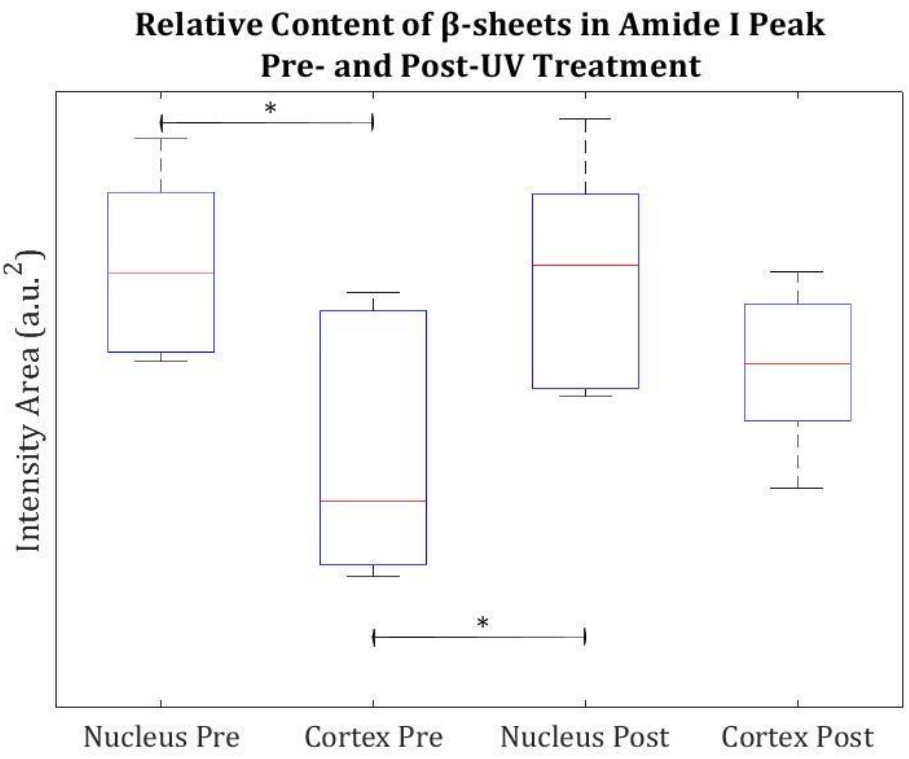

Figure 16: Comparison of β-sheet levels for the A1 peak in cortical and nuclear tissue. Right-tailed, equal variance, paired t-tests were conducted on the samples within treatments between tissues. Right-tailed, equal variance, two-sample t-tests were conducted on the samples between treatments. The levels of the nucleus β-sheets both pre- and post-treatment were significantly higher than the cortex pre-treatment ($p = 0.0345$ and 0.0316, respectively). While the difference post-treatment is not significantly larger for either pre- or post-treatment levels in the nucleus versus the cortex ($p = 0.0547$ and 0.1661, respectively), the trends are consistent with other reports.

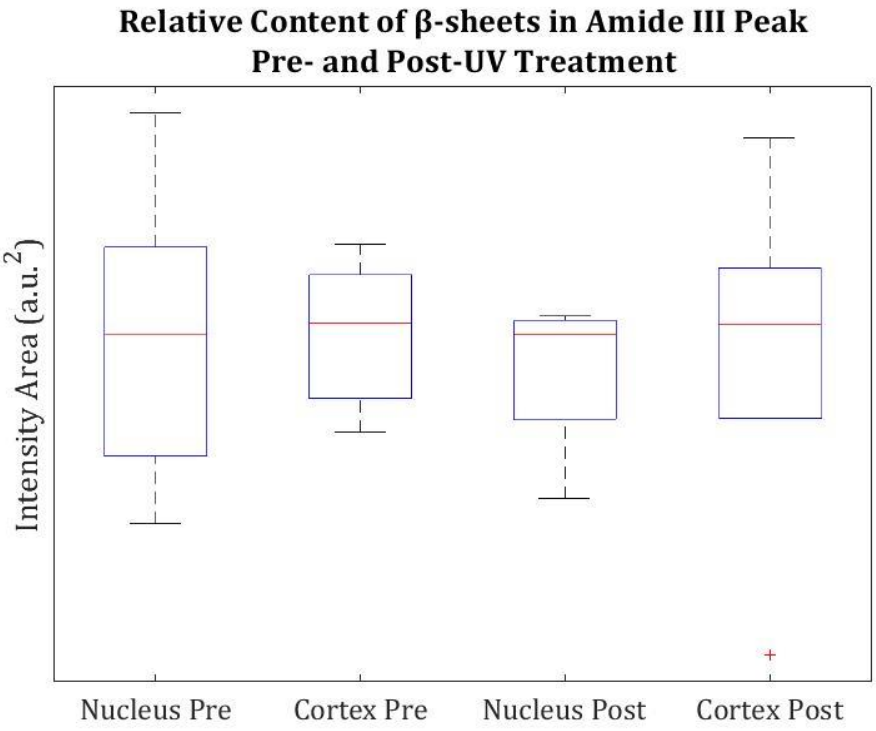

Figure 17: Comparison of β-sheet levels for the A3 peak in cortical and nuclear tissue. Right-tailed, equal variance, paired t-tests were conducted on the samples within treatments between tissues. Right-tailed, equal variance, two-sample t-tests were conducted on the samples between treatments. The differences are not significant, and it does not appear as if treatment has any effect on either tissue, although the cortex post-treatment has larger variance.

Neither treatment nor tissue showed many trends in differences in the tryptophan peak ratio, as shown in Figures 16 through 18. The treatment may reduce the amount of variation in the tissues. The average across tissues and treatments was ~0.72, which is concordant with literature values. This indicates the fitting program does not significantly alter the spectra, and the tissue samples are representative of other results with respect to tryptophan.

Figure 20 is the relative measured level of tryptophan content in lens protein tissue pre- and post-UV treatment. There are no statistically significant differences between treatments or within tissues. Despite there not being statistical significance, both tissues trended toward a lower value post-UV treatment.

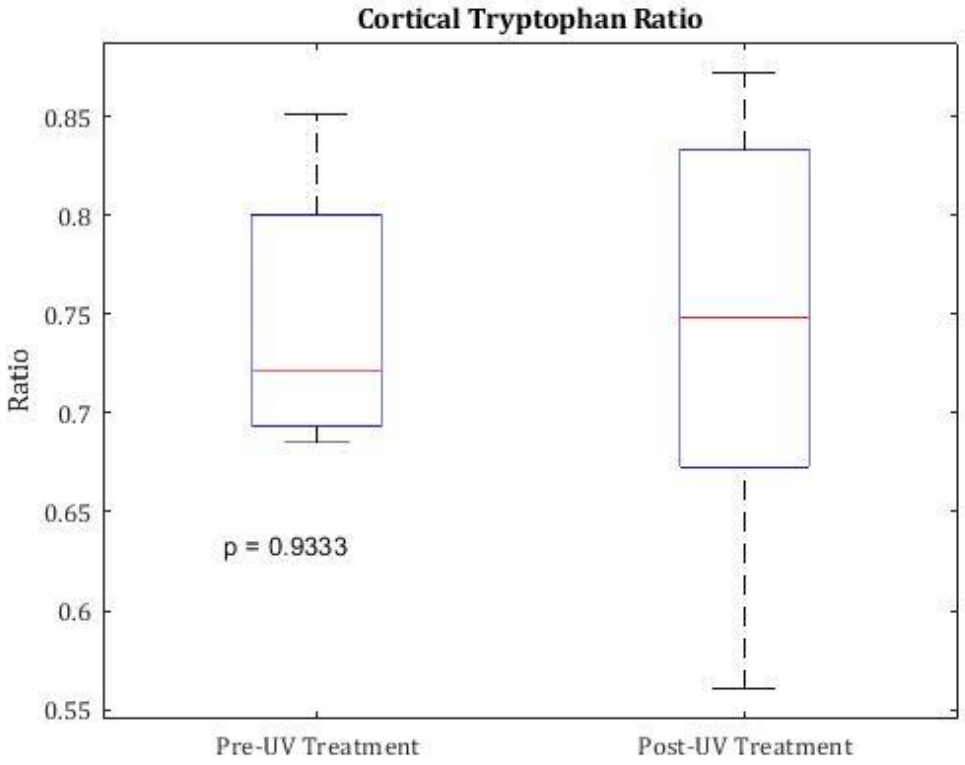

Figure 18: Comparison of the tryptophan ratio ($880cm^{-1}/760cm^{-1}$) for cortical tissue. The difference is not significant, the average slightly higher, but the deviations are very similar for post-treatment samples. However, the deviation is much larger in the post-treatment samples as well.

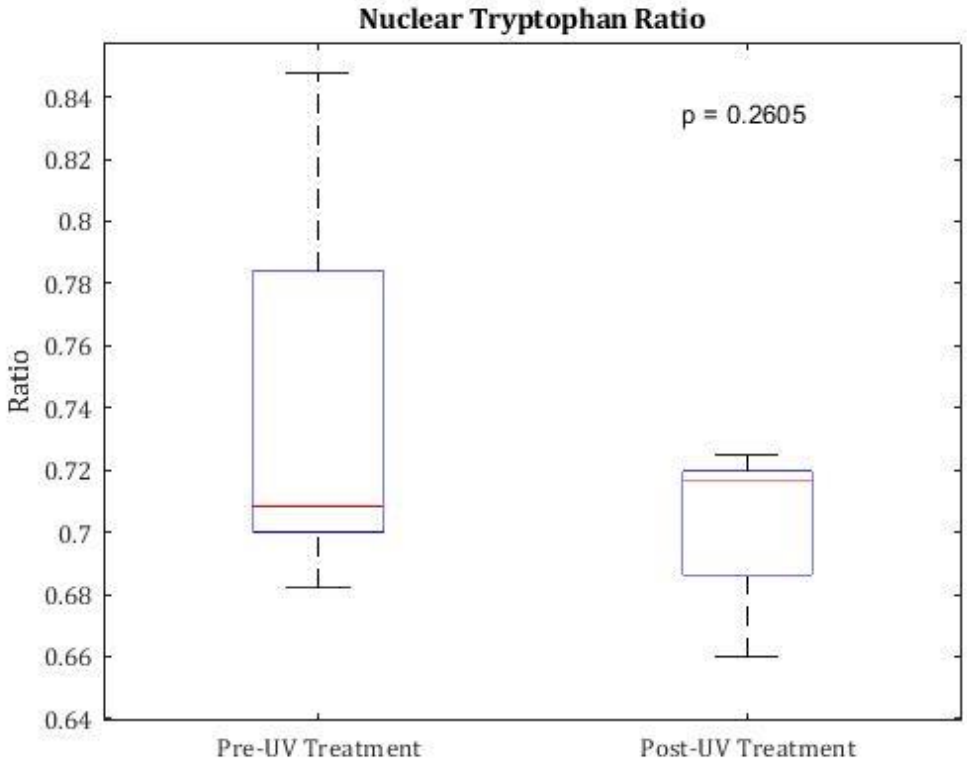

Figure 19: Comparison of the tryptophan ratio ($880cm^{-1}/760cm^{-1}$) for nuclear tissue. The difference is not significant, the average slightly higher, and the deviation slightly lower for post-treatment samples. While not statistically significantly different, the deviation for the pre-treatment samples was much larger.

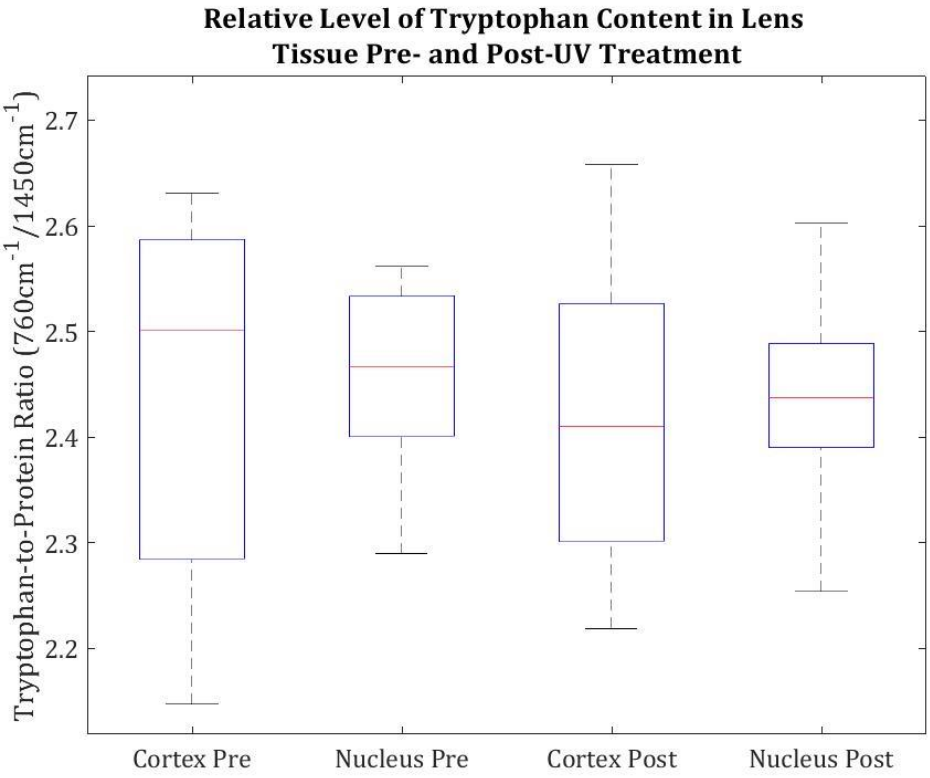

Figure 20: Relative measured level of tryptophan content in lens protein tissue ($880cm^{-1}/760cm^{-1}$) pre- and post-UV treatment. There are no statistically significant differences between treatments or within tissues, although both the nucleus and cortex trended lower post-UV treatment.

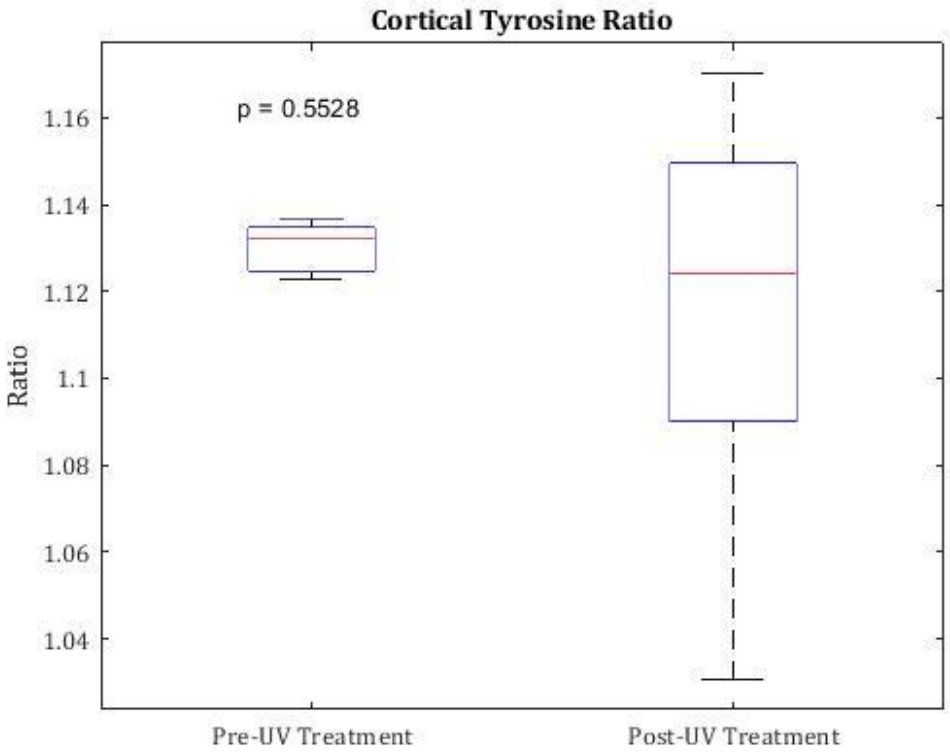

Figure 21: Comparison of the tyrosine ratio ($855cm^{-1}/830cm^{-1}$) for cortical tissue. The difference is not significant, the average slightly higher, but the deviations are much larger for post-treatment samples.

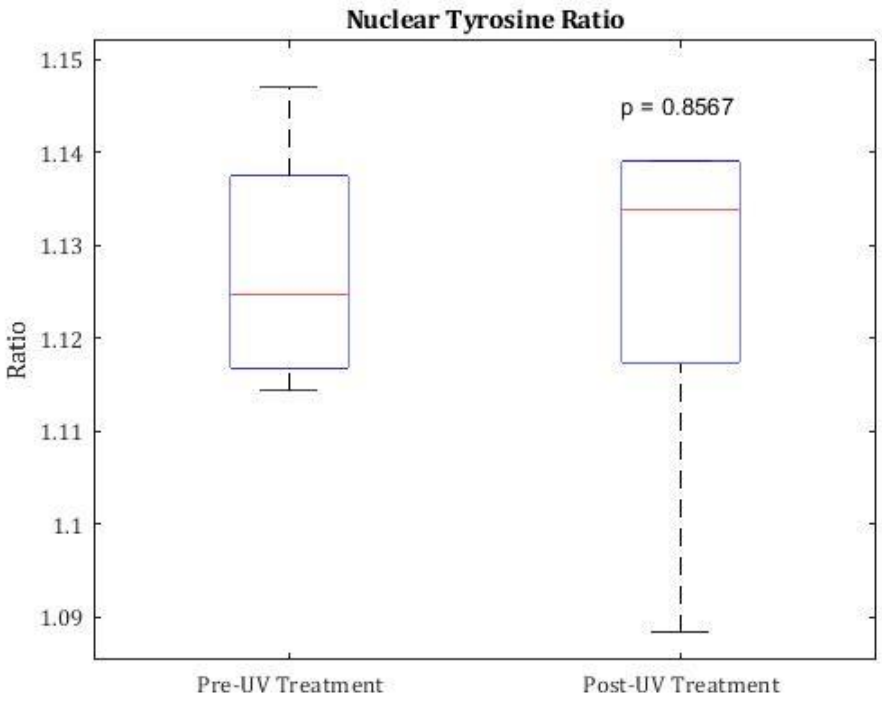

Figure 22: Comparison of the tyrosine ratio (855 cm^{-1}/830cm^{-1}) for nuclear tissue. The difference is not significant, the average slightly higher, but the deviations are larger for post-treatment samples.

Neither treatment nor tissue showed many trends in differences in the tyrosine peak ratio. Treatment may increase the amount of variation in the tissue. The average across tissues and treatments was ~1.13, which is concordant with literature values. This indicates the fitting program does not significantly alter the spectra, and the tissue samples are representative of other results with respect to tyrosine.

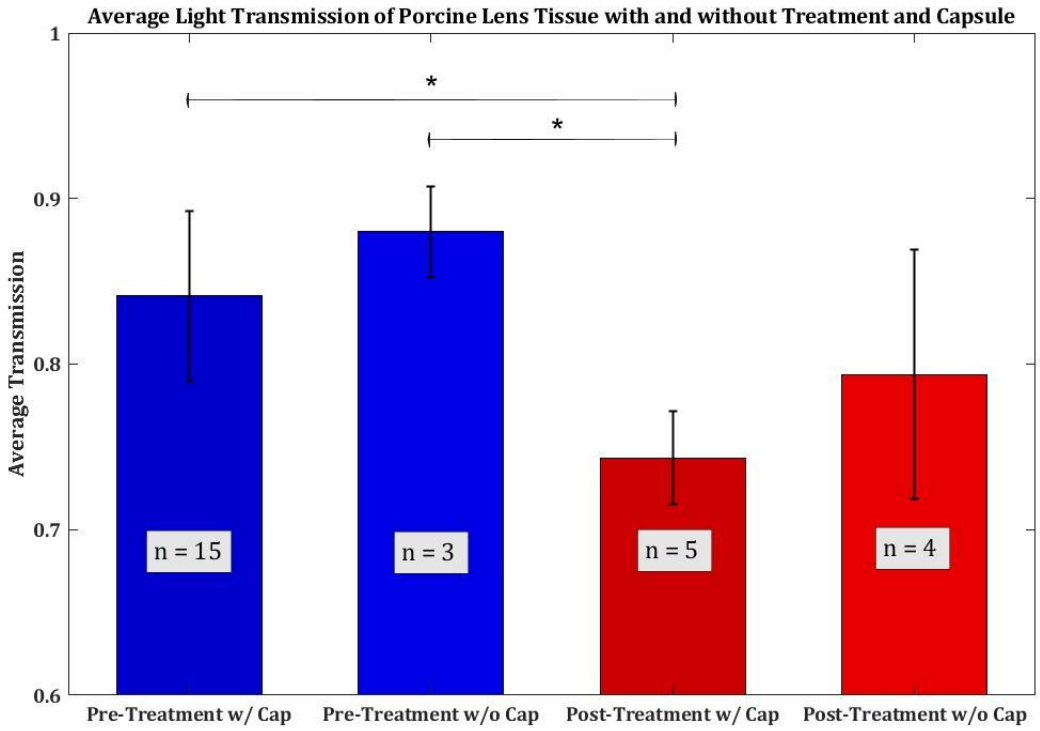

Figure 23: The average transmission for the lenses with capsule intact post-UV treatment were significantly lower according to a left-tailed t-test ($\alpha = 0.05$). However, this difference disappears when the capsule is removed, indicating the capsule may be undergoing opacification, as opposed to the lens itself. However, though not statistically significantly lower, the values for post-UV treatments lenses after capsule removal are lower on average.

The average visible light transmittance was measured across different samples. All post-UV treatment samples were represented in either or both pre-treatment groups. Capsule removal across all groups increased light transmission. T-tests revealed statistical differences between both pre-UV treatment groups and the post-UV treatment group with capsules intact. However, this statistical difference was not present between those same two groups and the post-UV treatment group with the capsules removed.

Although post-UV treatment groups can be examined with averages, qualitative analysis of the lenses revealed that some capsules and lenses opacified, while other samples had only the capsule opacify. Therefore, examining the post-UV treatment group without the capsule reveals that two samples “rebounded” in their transmission, while the other two retained their modified average transmission. The Raman spectra for these samples are displayed in Figure 24 and

Figure 25 and differences in the disulfide bonding, tyrosine, and tryptophan ratio of the opacified lens samples cortical tissue are shown in

Figure 26.

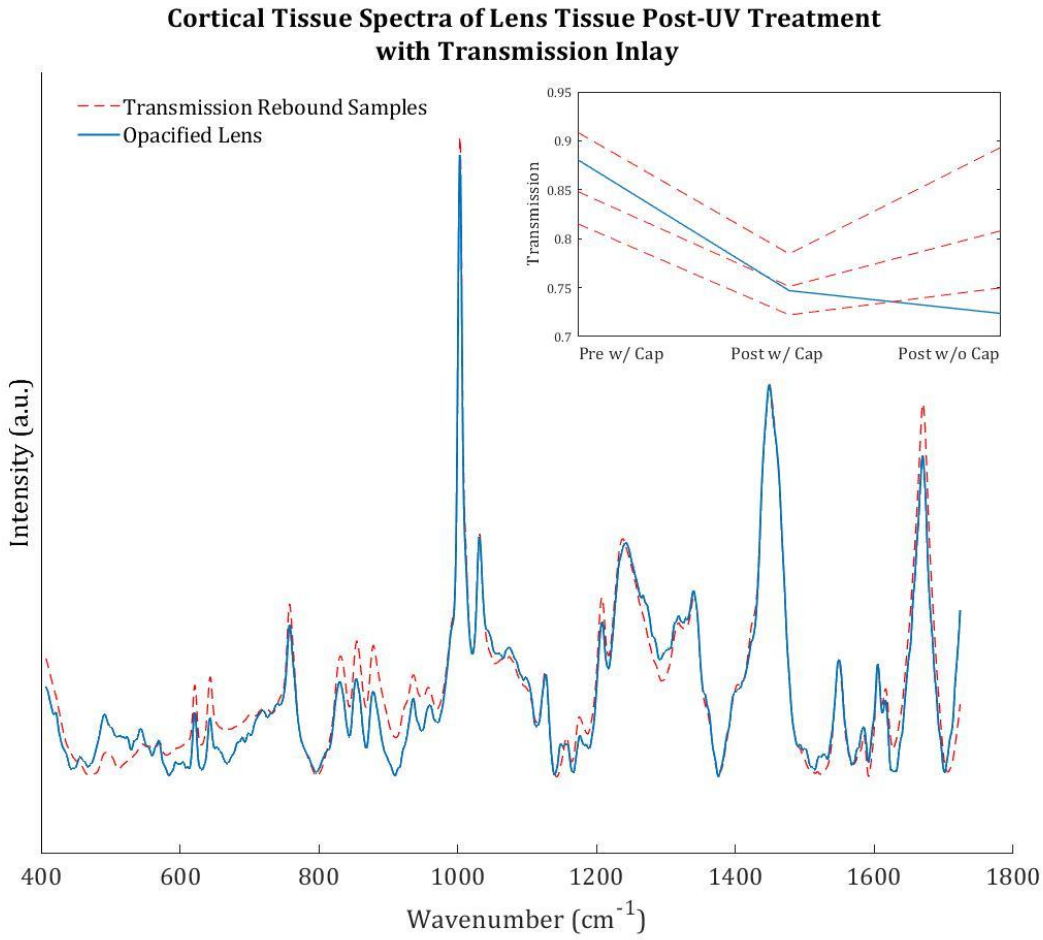

Figure 24: Raman spectra of cortical samples where measurements of opacity were taken before and after treatment. The samples that "rebounded" in transparency with removal of the capsule are plotted against the sample that did not (inset). Along with not regaining transparency with capsule removal (indicating opacification of the lens and not just the capsule), this sample also showed differences at many places in the spectrum, including in the tryptophan and tyrosine ratios as well as peak shifts in the A1 and A3 peaks. Another notable change is in the 500-600cm^{-1} region, which is associated with changes in sulfide bonding. Peaks around 500cm^{-1} indicate the presence of oxidized sulfide bonds, leading to disulfide bonds not originally present or between otherwise not typically bonded sulfurs.

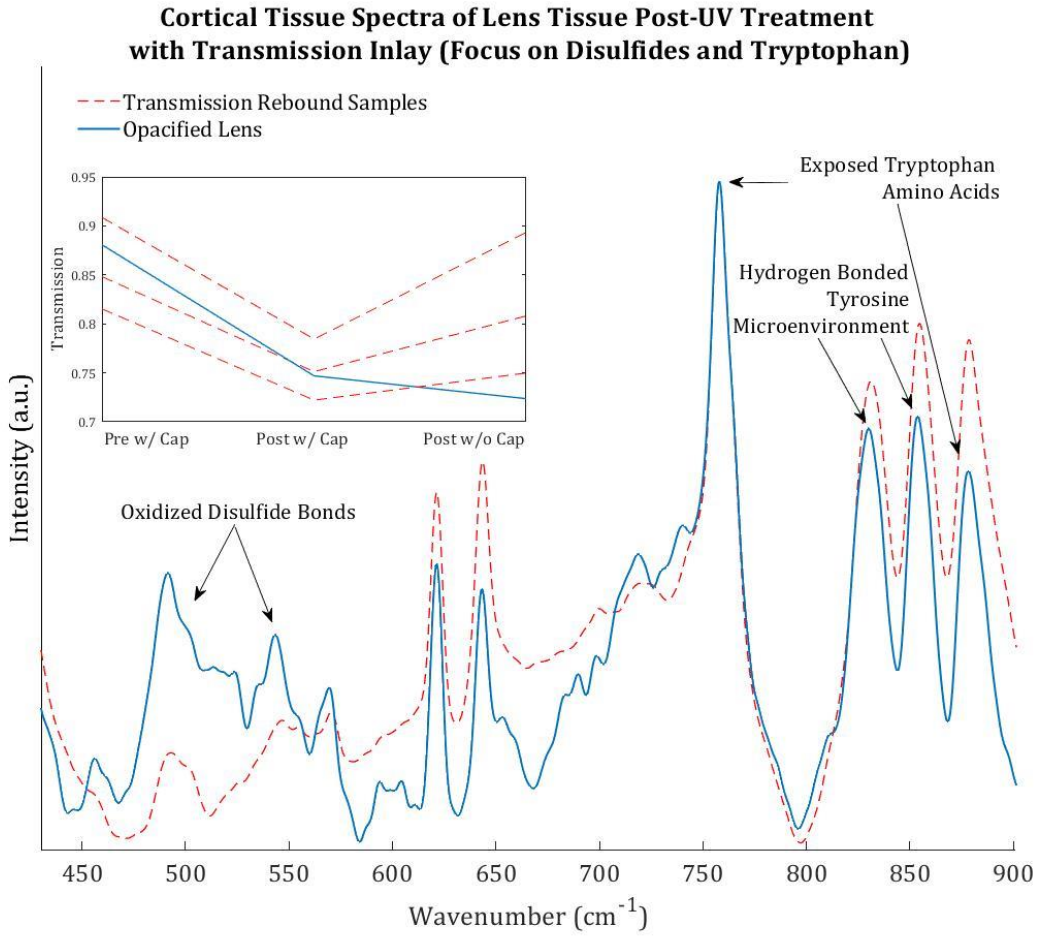

Figure 25: Close up on the disulfide, tyrosine, and tryptophan areas of interest of the cortical samples mentioned in Figure 24. The samples that "rebounded" in transparency with removal of the capsule are plotted against the sample that did not (inset). Along with a change in the tyrosine ratio (855 cm^{-1}/830cm^{-1}), the figure calls out the tryptophan peak that may be linked to an exposed and oxidized tryptophan amino acid. Also labeled on the figure is the presence of peaks at 500 cm^{-1} and 545 cm^{-1}. These peaks are indicative of sulfurs present that were oxidized and formed disulfide bonds. While disulfide bonds are present in lens proteins, other paper studies have shown that peaks of this nature indicate misfolding due to bonds between sulfurs that are not bound together in healthy, young lens tissue.

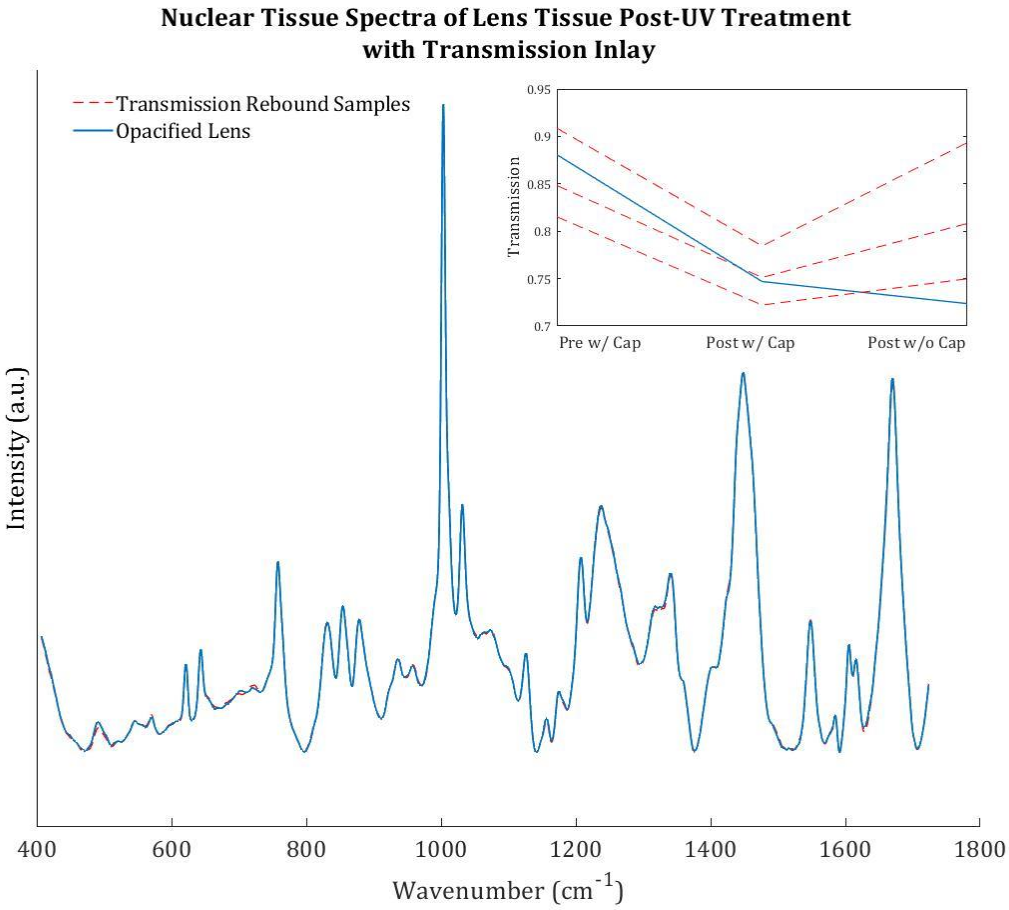

Figure 26: Raman spectra of cortical samples where measurements of opacity were taken before and after treatment. The samples that "rebounded" in transparency with removal of the capsule are plotted against the sample that did not (inset). Although the cortical sample showed difference in its spectrum (see Figure 24), the nucleus appears mostly unchanged among the samples. This may indicate that the changes incurred did not reach "as deep" as the nucleus, or that the nucleus is otherwise protected by changes of that magnitude.

Chapter 4: Discussion/Conclusions

Figure 11 and Figure 12 show that this method of peak deconvolution is more accurate than peak or intensity comparison methods of determining secondary protein content. This is the case as the peak deconvolution method is the only one that demonstrates differences between the nucleus and cortex that are expected based on what is known about these two types of tissues in the lens. While the small sample size resulted in trends which were not always statistically significant, the other methods investigated did not even produce the expected trends. Since the peak deconvolution program demonstrated more physiologically relevant trends, and recapitulated important knowledge, it can be considered a more reliable approach.

Based on the data, it is difficult to draw certain conclusions about the level of β-sheets and α-helices across the tissue types.

Figure 13 compares the fitting error for the cortical and nuclear tissues for the A1 and A3 peaks. While there is not significant difference within the peaks, the A3 peak is much more susceptible to variability in fitting.

The reason for this variability is likely due to the numerous components within the A3 peak of the lens [58]. Conversely, the A1 peak in the lens is dominated by a few protein conformations, notable the β-sheets peak around 1670cm^{-1}. This likely explains the relatively low fitting error for A1 and likely speaks to the reliability of the A1 peak in giving insight to the level of β-sheets and α-helices.

The difference in fitting may also have to do with the specific bond mode measured within each peak. While the A1 mode is characterized by a C=O stretch, the A3 is characterized by C-N stretch and N-H bend. This may indicate that the amide portions of the lens proteins are less affected by UV treatment, whereas the C=O portion, part of the protein backbone and likely involved in proper protein folding due to its polarity, may be susceptible to change [59]. This can be an important consideration in interpreting the effects of UV treatment.

In a report on A1 amide carbonyl stretching, it was hypothesized that an increasing peak height indicates C=O stretching that leads to a negative charge on the oxygen bonded to the carbon [60]. Although any sort of chemical interaction in such a complex environment may not be easy to predict, a negative charge may lead to

interactions between proteins. These interactions may be responsible for some of the misfolding presented for one theory of cataract formation and lens aging.

In total, it is difficult to interpret what the lack of statistically significant changes in the secondary protein mean. While certain trends are observed, some studies on color and cataract presence in different tissues do not show a difference in secondary protein levels [14] [61] [62] [63], while others observe that microenvironmental changes precede changes in secondary protein content, particularly β-sheet increase with deamidation [10] [64]. This study, at the very least, replicates some known aging effects found in other studies. Further studies should replicate other forms of aging and attempt to discern secondary protein content. It may be that only certain forms of aging incur changes in secondary protein content, and these changes may correlate in ARNC, even if there is no causative link. However, even if secondary proteins do not fully explain differences within treatment, other clues remain about the microenvironment and aging.

The results displayed in Figure 20 show trends, but nothing statistically significant. Results are controversial as for whether tryptophan is increased or decreased with lens age [61] [65]. While this the current experiment does not seek to make authoritative statements in this regard, it does show that the relative tryptophan content, normalized for total protein content, appears to decrease with UV treatment.

While the samples largely did not change between treatment and tissue types for most of the other observed aspects of the lens, one cortical sample underwent change that resulted in true opacification of the lens as well as changes to the disulfide, tyrosine, and tryptophan microenvironments.

According to

Figure 25, cortical lens tissue associated with true lens opacification (no rebound in light transmission after removal of the capsule) underwent many microenvironment changes. While this sample did not have out of the ordinary differences in its relative α-helix or β-sheet content, following the same trends as other samples, other changes were noticeable in the Raman spectrum.

First, the peaks at $500cm^{-1}$ and $550cm^{-1}$ were much more distinct, indicating oxidation of sulfides that may lead to disulfide bonding [7]. This disulfide bonding is only partially reversible, but importantly may lead to irreversible bonding and "locking" of proteins together in a misfolded shape [21]. Worse yet, this process seems to be at least semi-random in that these disulfide bonds can be switched between four various sulfides within lens proteins, and if the wrong pair is linked, it initiates a cascade effect that leads to "kinks" in other copies of the protein. Therefore, while disulfide bonds exist naturally within a healthy lens, the prominence of these peaks indicate, according to other studies, a change in the disulfide environment. This may be linked to this runaway process. This lends weight to the hypothesis that disulfide bonding may be linked to lens opacification, and may also be associated with lens aging.

Second, the ratio of tryptophan peaks of $880cm^{-1}/760cm^{-1}$ indicate a change in the microenvironment that may be linked to exposure and oxidation of the tryptophan protein [47]. Studies have been done on cold, diabetic, genetically induced, and hereditary cataracts which all indicate this change occurring [12] [17] [47] [66]. Notably, the levels

observed on average all correlate with levels in humans (~0.72) [65]. However, while this level has been observed to decrease with cataract formation, other studies show its decrease related more to aging [15] [61] [66]. However, as stated earlier, this is controversial in studies not all being concordant. One aspect to keep in mind is that this ratio may be affected by deamidation, and this deamidation is largely an age-related phenomenon and therefore may not be the same across species or animal groups. The current study indicates that changes in the tryptophan ratio, likely linked to exposure, oxidation, and further hydrogen bonding at various tryptophan residues is linked with lens opacification.

Third, the tyrosine ratio of $855cm^{-1}/830cm^{-1}$ shows a marked decrease in this sample versus the average. Again, noting that the ratio observed is typical in the other samples, even post-UV treatment, it is remarkable that the ratio observed is much closer to the ratio expected in other types of cataract and aging [15] [17] [47] [66]. This decrease in ratio is also correlated with water content, due to the nature of the hydrogen bonding that may occur with the tyrosine. This leads to the hypothesis that lens opacification is linked with a drop in this ratio. The current study shows a very sharp decrease in this ratio with this opacified sample and supports that hypothesis.

What is less clear is why only one of five samples changed so greatly with UV treatment, while the other samples remained unaltered. It is easy enough to explain the difference between the nucleus and cortex in treatment by saying that the nucleus was insulated against oxidation and other induced aging factors. The cortex, being the newer

proteins surrounding the older core, are obviously more susceptible to change. Why some cortical samples remained “healthier” than others, though, is the question.

As with most biological questions, the answer likely has to do with a host of factors, including age, genetic predisposition, and other traumas and insults inflicted on the eye and lens prior to experimentation. Other studies also showed that one-off events can lead to cascading problems, and the issue with cascading events in biology is well known. Therefore, we conclude that the UV treatment induced damage in all of the samples, while one sample was particularly impacted due to the experimental conditions of both the sample and testing apparatus. However, one in five samples being affected is not a result from which statistical probability may be drawn. While this study is largely experimental and without precedent, it would also be unfair to say that the observed results are completely random. Rather, the one sample likely reflects a possible outcome that has been observed in the literature occurring across species, experiments, treatments, and age. Further experiments should attempt to recreate this process reliably and then winnow out the factors that are unimportant.

One question of lens aging that lingers is how other components of the lens changes with age. While there are some aspects not suited to Raman spectroscopy, or other light spectroscopy techniques, there are some questions that can at least be investigated with Raman spectroscopy. This includes questions about lens lipid and carbohydrate content, both of which have important implications in lens health [67] [68]. Other theories of lens aging and cataractogenesis implicate lipids and carbohydrate interactions, and there have been attempts to analyze these interactions [69] [70] [71].

Lipid and carbohydrates have already been characterized in Raman spectroscopy; the next step would be aligning the known spectra with biologically relevant peaks and characteristics [72] [73].

Limitations

One assumption in this study is that young porcine lenses are biochemically identical. Among the attributes that affect this homogeneity are age, ocular trauma, post-translational modifications (which may be random, genetic, or environmental), and chance. The samples obtained for this study are from a local abattoir, but that abattoir is a wholesale supplier of pork products, and the age of the samples may reflect different needs of the various buyers. Even if age can be controlled, however, the other factors remain uncontrolled.

Another assumption in this study is that non-opacified lenses after the preconditioning period still have living lens epithelial cells (LECs). LECs facilitate lens fiber growth, regulate nutrients in the lens environment, and generate important proteins, like the α-crystallin chaperones discussed previously [74]. As stated in the methodology, lenses were assumed to be "healthy" when the lens showed relatively little opacification. This opacification can be observed in the lens when it is damaged or care is not taken to preserve the lens capsule during extraction. For that reason, if the lens does not show opacification after extraction, it was assumed that the LECs were alive and able to maintain the appropriate cellular environment for light refraction and cell maintenance. However, no measurements were conducted during this study to assess LEC health. If the

LECs are not alive, then pathological changes may occur during the preconditioning period.

The preconditioning media is a combination of M199 with antibiotics, glutamine, and antifungal components. The preconditioning period involves incubation at 37°C and a relatively inert environment. However, this period of conditioning does not involve inclusion of other features specific to the eye, such as the vitreous, cyclic and sustained stress from the zonule fibers, and the cornea and scleral protection afforded to the lens. These missing components may alter the health of the LECs and lens proteins, which in turn may affect the state of the protein of the lens.

Another major assumption resides within the operation of the peak fitting program itself. While care was taken in the design, development, and implementation of the fitting program, the problem remains that there are occasionally times where manual peak assignment was required. This was especially an issue in the A3 peak where the peak assigned to the area between 1265 and 1275cm^{-1} was often lower in wavenumber than expected. In these cases, the content of the α-helix of the A3 band is potentially skewed. Also, the peak fitting is sequentially iterative and based on fitting the best RMS error. Fitting of this type is limited by granularity limits and computing power on top of allowable tolerance and limits in the data. In this case, iterative fitting fit both peak width and peak position, but only within five wavenumber of each. Therefore, if a better-fit peak were available outside of the iteration, it would not have been found. The sequential nature of the peak fitting also means that each peak is approached in order, from lower to higher wavenumber, and fitting parameters in one peak is carried over to the next.

The most glaring limitation, and likely the biggest problem with human lens research today and likely into the future, is the equitability of the animal models [75]. Truscott, a vocal proponent of molecular modifications being the key to ARNC and aging, argues that no suitable animal models exist for ARNC due to lack of aging models and similarity with humans. Not only do many of the studies cited in this experiment use non-primate, non-human animal models, but the type of animal tends to vary from mouse to rabbit to guinea pig. When humans are involved, there are many limitations, like age and disease condition, and many unknowns cast doubt on definitive conclusions. This study, no different, focuses on porcine lenses, possibly introducing systematic biases.

Future Work

Subsequent studies would benefit from an increased sample size. The amount of samples in the current work is a good baseline for validating the program and making a first-pass look at some aging and pathology mechanisms related to UV radiation, the seemingly stochastic nature of cataract location and formation may be better pinned down with more testing.

Another improvement would be a shift from total spectrum UV (100-400nm) to UV-B (280-315nm), which is hypothesized to be the most physiologically relevant spectrum in protein change and cataract development [39] [76] [77] [78]. UV-B may be linked to cleaving proteins and other types of protein conformation change, and therefore may be an important factor in UV-radiation type cataractogenesis [79]. Also, the chosen power of $1W/cm^2$ is an arbitrary level, and so studying changes in dose level and exposure time is valuable. It may also be that the use of broad-spectrum UV caused non-

physiologic changes in proteins, potentially accounting for the lack of expected trends in the data.

The program developed can also be used with other treatments, such as hydrogen peroxide exposure, which can help elucidate the effects of a different, but also physiologically relevant, ageing mechanism [80]. While the results are mixed here and in the literature on the changes to secondary proteins with ageing and cataract formation, oxidation mechanisms have not been assessed *in vitro* in a quantifiable way without destruction of the tissue.

Subsequent studies should also measure the differences in WS and WI proteins. There could be important differences in protein distribution, response, and absolute amounts between these two types of protein in the lens, and observing how they change with age and oxidation mechanisms can help explain why there may be some asymmetries. The same thinking can also be expanded to lipids in the lens, which serve an important function [67].

Lastly, the program can be used to form a baseline in human lenses and observe the differences in the human lens with ageing versus a young porcine lens. This can help illustrate the differences in both ageing and species with regard to the various features measured here.

Chapter 5: References

[1] V. L. Taylor, K. J. Al-Ghoul, C. W. Lane, V. A. Davis, J. R. Kuszak and M. J. Costello, "Morphology of the Normal Human Lens," *Investigative Ophthalmology & Visual Science,* vol. 37, no. 7, pp. 1396-1410, June 1996.

[2] R. Michael and A. J. Bron, "The ageing lens and cataract: a model of normal and pathological ageing," *Philosophical Transactions of the Royal Society B,* vol. 366, no. 1568, pp. 1278-1292, 27 April 2011.

[3] R. Truscott, "Age-related nuclear cataract-oxidation is the key," *Experimental Eye Research,* pp. 709-725, 2005.

[4] C.-C. Huang and C. Wenlung, "Raman spectroscopic analysis of cataract lens: A compendious review," *Applied Spectroscopy Review,* vol. 53, no. 9, pp. 689-702, 2018.

[5] I. López-Peña, B. S. Leigh, D. E. Schlamadinger and J. E. Kim, "Insights into Protein Structure and Dynamics by Ultraviolet and Visible Resonance Raman Spectroscopy," *Biochemistry,* vol. 54, no. 31, pp. 4770-4783, 2015.

[6] A. Elliott and E. J. Ambrose, "Structure of Synthetic Polypeptides," *Nature,* vol. 165, no. 4206, pp. 921-922, 1950.

[7] C.-H. Wang, C.-C. Huang, L.-L. Lin and W. Chen, "The effect of disulfide bonds on protein folding, unfolding, and misfolding investigated by FT–Raman Spectroscopy," *Journal of Raman Spectroscopy,* 2016.

[8] G. F. J. M. Vrensen, C. Otto, A. Lenferink, B. Liszka, G. A. Montenegro, R. I. Barraquer and R. Michael, "Protein profiles in cortical and nuclear regions of aged human donor lenses: A confocal Raman microspectroscopic and imaging study," *Experimental Eye Research,* vol. 145, pp. 100-109, 2016.

[9] Z. Zhuang, M. Zhu, Y. Huang, J. Liu, Z. Guo, K. Xiong, N. Li, S. Chen and X. Qiu, "Study of molecule variation in various grades of human nuclear cataracts by confocal micro-Raman spectroscopy," *Applied Physics Letters,* vol. 101, no. 17, 2012.

[10] J. Sacharz, A. Weselucha-Birczynska, C. Paluszkiewicz, P. Chaniecki and M. Blazewicz, "A 2D correlation Raman spectroscopy analysis of a human cataractous lens," *Journal of Molecular Science,* vol. 1124, pp. 71-77, 2016.

[11] H. J. Tweeddale, C. L. Hawkins, J. F. Janmie, R. J. Truscott and M. J. Davies, "Cross-linking of lens crystallin proteins induced by tryptophan metabolites and metal ions: implications for cataract development," *Free Radical Research,* vol. 50, no. 10, pp. 1116-1130, 2016.

[12] K. Itoh, Y. Ozaki, A. Mizuno and K. Iriyama, "Structural changes in the lens proteins of hereditary cataracts monitored by Raman spectroscopy," *Biochemistry,* vol. 22, no. 8, pp. 1773-1778, 1983.

[13] I. M. Streete, J. F. Jamie and R. J. Truscott, "Lenticular Levels of Amino Acids and Free UV Filters Differ Significantly between Normals and Cataract Patients," *Investigative Ophthalmology & Visual Science,* vol. 45, pp. 4091-4098, November 2004.

[14] I. Siebinga, G. F. Vrensen, K. Otto, G. J. Puppels, F. F. De Mul and J. Greve, "Ageing and Changes in Protein Conformation in the Human Lens: A Raman Microspectroscopic Stud," *Experimental Eye Research,* no. 54, pp. 759-767, 1992.

[15] Z. Zhuang, M. Zhu, Y. Huang, J. Liu, Z. Guo, K. Xiong, N. Li, S. Chen and X. Qiu, "Study of molecule variation in various grades of human nuclear cataracts by confocal micro-Raman spectroscopy," *Applied Physics Letters,* vol. 101, no. 17, 2012.

[16] A. Mizuno, H. Nishigori and M. Iwatsuru, "Glucocorticoid-induced cataract in chick embryo monitored by Raman spectroscopy," *Investigative Ophthalmology & Visual Science,* vol. 30, no. 1, pp. 132-137, 1989.

[17] A. Mizuno, Y. Ozaki, K. Itoh, S. Matsushima and K. Iriyama, "Raman spectroscopic evidence for the microenvironmental change of some tyrosine residues of lens proteins in cold cataract," *Biochemical and Biophysical Research Communications,* vol. 119, no. 3, pp. 989-994, 1984.

[18] Y. Ozaki, A. Mizuno, K. Itoh, M. Yoshiura, T. Iwamoto and K. Iriyama, "Raman spectroscopic study of age-related structural changes in the lens proteins of an intact mouse lens," *Biochemistry,* vol. 22, no. 26, pp. 6254-6259, 1983.

[19] C. Paluszkiewicz, P. Chaniecki, M. Rekas, B. Rajchel, N. Piergies and W. Kwiatek, "Analysis of Human Lenses by Raman Microspectroscopy," *Acta Physica Polonica A,* vol. 129, no. 2, pp. 244-246, 2016.

[20] R. Truscott, "Age-Related Nuclear Cataract: A Lens Transport Problem," *Opthalmic Research,* vol. 32, no. 5, pp. 185-194, 2000.

[21] E. Serebryany, S. Yu, S. A. Trauger, B. Budnik and E. I. Shaknovich, "Dynamic disulfide exchange in a crystallin protein in the human eye lens promotes cataract-associated aggregation," *Journal of Biological Chemistry,* vol. 293, no. 46, pp. 17997-18009, 2018.

[22] E. Serebryany, J. C. Woodard, B. V. Adkar, M. Shabab, J. A. King and E. I. Shakhnovich, "An Internal Disulfide Locks a Misfolded Aggregation-Prone Intermediate in Cataract-Linked Mutants of Human Gamma-D Crystallin," *Biophysical Journal,* vol. 112, no. 3, pp. 167a-168b, 2017.

[23] R. J. W. Truscott and M. G. Friedrich, "Molecular Processes Implicated in Human Age-Related Nuclear Cataract," *Investigative Ophthalmology & Visual Science,* vol. 60, no. 15, pp. 5007-5021, 2019.

[24] N.-T. Yu, D. C. DeNagel, P. L. Pruett and J. F. Kuck Jr., "Disulfide bond formation in the eye lens," *Proceedings of the National Academy of Science USA 82: Biochemistry,* vol. 82, pp. 7965-7968, 1985.

[25] D. Boyle and L. Takemoto, "Characterization of the alpha-gamma and alpha-beta Complex: Evidence for an In Vivo Functional Role of alpha-Crystallin as a Molecular Chaperone," *Experimental Eye Research,* vol. 58, no. 1, pp. 9-16, 1994.

[26] H. Bloemendal, W. d. Jong, R. Jaenicke, N. H. Lubsen, C. Slingsby and A. Tardieu, "Ageing and vision: structure, stability and function of lens crystallins," *Progress in Biophysics and Molecular Biology,* vol. 86, no. 3, pp. 407-785, 2004.

[27] S. Su, P. Liu, H. Zhang, Z. Li, Z. Song and S. Chen, "Proteomic Analysis of Human Age-related Nuclear Cataracts and Normal Lens Nuclei," *Investigative Ophthalmology & Visual Science,* vol. 52, pp. 4182-4191, 2011.

[28] J. Keenan, B. K. Pierscionek and D. F. Orr, "Patterns of crystallin distribution in porcine eye lenses," *Molecular Vision,* vol. 14, pp. 1245-1253, 2008.

[29] J. A. Carver, K. A. Nicholls, A. J. Aquilina and R. J. W. Truscott, "Age-related Changes in Bovine α-crystallin and High-molecular-weight Protein," *Experimental Eye Research,* vol. 63, no. 6, pp. 639-647, 1996.

[30] P. Zelenka and J. Piatigorsky, "Isolation and In Vitro Translation of δ-Crystallin mRNA from Embryonic Chick Lens Fibers," *Proceedings of the National Academy of Sciences of the United States of America,* vol. 71, no. 5, pp. 1896-1900, 1974.

[31] K. L. Moreau and J. A. King, "Protein Misfolding and Aggregation in Cataract Disease and Prospects for Prevention," *Trends in Molecular Medicine,* vol. 18, no. 5, pp. 273-282, May 2012.

[32] K. R. Heys, M. G. Friedrich and R. J. Truscott, "Presbyopia and heat: changes associated with aging of the human lens suggest a functional role for the small heat shock protein, alpha-crystallin, in maintaining lens flexibility," *Aging Cell,* vol. 6, pp. 807-815, 2007.

[33] S. Lindquist and E. A. Craig, "The Heat-Shock Proteins," *Annual Review of Genetics,* vol. 22, pp. 637-677, 1988.

[34] P. G. Hains and R. J. W. Truscott, "Proteome analysis of human foetal, aged and advanced nuclear cataract lenses," *Proteomics - Clinical Applications,* vol. 2, no. 12, pp. 1611-1619, 2008.

[35] C. Asomugha and O. Srivastava, "Identification of crystallin modifications in the human lens cortex and nucleus using laser capture microdissection and CyDye labeling," *Molecular Vision,* vol. 16, pp. 476-494, 2010.

[36] W. Graeme, "The human crystallin gene families," *Human Genomics,* vol. 6, no. 26, pp. 1-10, 2012.

[37] P. H. Frederikse, "Amyloid-like protein structure in mammalian ocular lenses," *Current Eye Research,* vol. 20, no. 6, pp. 462-468, 2000.

[38] N. T. Yu and E. J. East, "Laser Raman spectroscopic studies of ocular lens and its isolated protein fractions.," *Journal of Biological Chemistry,* vol. 250, no. 6, pp. 2196-2202, 1975.

[39] S. Cetinel, V. Semenchenko, J.-Y. Cho, M. G. Sharaf, K. F. Damji, L. D. Unsworth and C. Montemango, "UV-B induced fibrillization of crystallin protein mixtures," *PLOS One,* vol. 12, no. 5, 2017.

[40] V. Harrington, S. McCall, S. Huynh, K. Srivastava and O. P. Srivastava, "Crystallins in water soluble-high molecular weight protein fractions and water insoluble protein fractions in aging and cataractous human lenses," *Molecular Vision,* vol. 10, pp. 476-489, 2004.

[41] I. Siebinga, G. F. J. M. Vrensen, F. F. M. De Mul and J. Greve, "Age-related changes in local water and protein content of human eye lenses measured by Raman microspectroscopy," *Experimental Eye Research,* vol. 53, no. 2, pp. 233-239, 1991.

[42] A. Huizinga, A. C. Bot, F. F. De Mul, G. F. Vrensen and J. Greve, "Local Variation in Absolute Water Content of Human and Rabbit Eye Lenses Measured by Raman Microspectroscopy," *Experimental Eye Research,* vol. 48, pp. 487-496, 1989.

[43] P. Vandenabeele, Practical Raman Spectroscopy - An Introduction, Chichester: Wiley, 2013.

[44] Horiba, "Raman Spectroscopy," 2019. [Online]. Available: https://www.horiba.com/en_en/raman-imaging-and-spectroscopy/.

[45] J. L. Lippert, D. Tyminski and P. J. Desmeules, "Determination of the secondary structure of proteins by laser Raman spectroscopy," *Journal of the American Chemical Society,* vol. 98, no. 22, pp. 7075-7080, 1976.

[46] M. Berjot, J. Marx and A. J. P. Alix, "Determination of the secondary structure of proteins from the Raman amide I band: The reference intensity profiles method," *Journal of Raman Spectroscopy,* vol. 18, pp. 289-300, 1987.

[47] Y. Ho and F.-Y. Huang, "Raman Spectroscopy of Galactosemic Rat Lens Crystalline: Correlation of Microscopic Changes of Lens Proteins at Molecular Levels with Gross Cataractous Alteration," *Journal of the Chinese Chemical Society,* vol. 49, no. 2, pp. 283-290, 2002.

[48] M. Palencia, "Functional transformation of Fourier-transform mid-infrared spectrum for improving spectral specificity by simple algorithm based on wavelet-like functions," *Journal of Advanced Research,* pp. 53-62, 2018.

[49] I. Durickovic, "Using Raman Spectroscopy for Characterization of Aqueous Media and Quantification of Species in Aqueous Solution," *Applications of Molecular Spectroscopy to Current Research in the Chemical and Biological Sciences,* 2016.

[50] G. Vedantham, H. G. Sparks, S. U. Sane, S. Tzannis and T. M. Przybycien, "A Holistic Approach for Protein Secondary Structure Estimation from Infrared Spectra in H2O Solutions," *Analytical Biochemistry,* vol. 285, no. 1, pp. 33-49, 2000.

[51] S. M. Ali, F. Bonnier, H. Lambkin, K. Flynn, V. McDonagh, C. Healy, T. C. Lee, F. M. Lyng and H. J. Byrne, "A comparison of Raman, FTIR and ATR-FTIR micro spectroscopy for imaging human skin tissue sections," *Analytical Methods,* vol. 5, no. 9, pp. 2281-2291, 2013.

[52] M. R. Kagan and R. L. McCreery, "Reduction of Fluorescence Interference in Raman Spectroscopy via Analyte Adsorption on Graphitic Carbon," *Analytical Chemistry,* vol. 66, no. 23, pp. 4159-4165, 1994.

[53] T. O'Haver, "ipf(arg1,arg2,arg3,arg4)," MATLAB Central File Exchange, 2018.

[54] J. R. Kuszak, R. K. Zoltoski and C. E. Tiedemann, "Development of lens sutures," *The International Journal of Developmental Biology,* no. 48, pp. 889-902, 2004.

[55] Malvern Panalytical, Malvern.

[56] C. Lieber and A. Mahadevan-Jansen, "Automated method for subtraction of fluorescence from biological Raman spectra," *Applied Spectroscopy,* vol. 57, no. 11, pp. 1363-1367, 2003.

[57] MathWorks, "MATLAB," Natick, 2020.

[58] A. Rygula, K. Majzner, K. M. Marzec, A. Kaczor, M. Pilarczyk and M. Baranska, "Raman spectroscopy of proteins: a review," *Journal of Raman Spectroscopy,* vol. 44, no. 8, pp. 1061-1076, 2013.

[59] A. Moran and S. Mukamel, "The origin of vibrational mode couplings in various secondary structural motifs of polypeptides," *Proceedings of the National Academy of Sciences,* vol. 101, no. 2, pp. 506-510, 2004.

[60] W. C. Price, R. D. B. Fraser and W. T. Astbury, "Infra-red dichroism and protein structure," *Proceedings of the Royal Society of London. Series B - Biological Sciences,* vol. 141, no. 902, pp. 66-67, 1953.

[61] S. Nie, K. L. Bergbauer, J. F. R. Kuck and N.-T. Yu, "Near-infrared Fourier transform Raman spectroscopy in human lens research," *Experimental Eye Research,* vol. 51, no. 5, pp. 619-623, 1990.

[62] R. Michael, C. Otto, A. Lenferink, E. Gelpi, G. A. Montenegro, J. Rosandic, F. Tresserra, R. I. Barraquer and G. F. J. M. Vrensen, "Absence of amyloid-beta in lenses of Alzheimer patients: A confocal Raman microspectroscopic study," *Experimental Eye Research,* vol. 119, pp. 44-53, 2014.

[63] A. Pande, N. Mokhor and J. Pande, "Deamidation of Human γS-Crystallin Increases Attractive Protein Interactions: Implications for Cataract," *Biochemistry,* vol. 54, no. 31, pp. 4890-4899, 2015.

[64] T. O. Zhang, A. M. Alperstein and M. T. Zanni, "Amyloid β-Sheet Secondary Structure Identified in UV-Induced Cataracts of Porcine Lenses using 2D IR Spectroscopy," *Journal of molecular biology,* vol. 429, no. 11, pp. 1705-1721, 2017.

[65] M. H. Smeets, G. F. J. M. Vrensen, K. Otto, G. J. Puppels and J. Greve, "Local variations in protein structure in the human eye lens: a Raman microspectroscopic study," *Biochimica et Biophysica Acta (BBA) - Protein Structure and Molecular Enzymology,* vol. 1164, no. 3, pp. 236-242, 1993.

[66] Y. Ozaki, A. Mizuno, K. Itoh, S. Matsushima and K. Iriyama, "Raman Spectroscopic Study of Cataract Formation: Emory Mouse Cataract," *Applied Spectroscopy,* vol. 41, no. 4, pp. 597-605, 1987.

[67] D. Borchman and M. C. Yappert, "Lipids and the ocular lens," *Journal of Lipid Research*, vol. 51, no. 9, pp. 2473-2488, 2010.

[68] C.-J. Chiu, L. Robman, C. A. McCarty, B. N. Mukesh, A. Hodge, H. R. Taylor and A. Taylor, "Dietary Carbohydrate in Relation to Cortical and Nuclear Lens Opacities in the Melbourne Visual Impairment Project," *Investigative Ophthalmology & Visual Science*, vol. 51, no. 6, pp. 2897-2905, 2010.

[69] H. Sato, D. Borchman, Y. Ozaki, O. P. Lamba, C. W. Byrdwell, M. C. Yappert and C. A. Paterson, "Lipid –Protein Interactions in Human and Bovine Lens Membranes by Fourier Transform Raman and Infrared Spectroscopies," *Experimental Eye Research*, vol. 62, no. 1, pp. 47-54, 1996.

[70] D. Borchman, O. P. Lamba, Y. Ozaki and M. Czarnecki, "Raman structural characterization of clear human lens lipid membranes," *Current Eye Research*, vol. 12, no. 3, pp. 279-284, 1993.

[71] S.-Y. Lin, M.-J. Li, R.-C. Liang and S.-M. Lee, "Non-destructive analysis of the conformational changes in human lens lipid and protein structures of the immature cataracts associated with glaucoma," *Spectrochimica Acta Part A: Molecular and Biomolecular Spectroscopy*, vol. 54, no. 10, pp. 1509-1517, 1998.

[72] K. Czamara, K. Majzner, M. Z. Pacia, K. Kochan, A. Kaczor and M. Baranska, "Raman spectroscopy of lipids: a review," *Journal of Raman Spectroscopy*, vol. 46, no. 1, pp. 4-20, 2015.

[73] E. Wiercigroch, E. Szafraniec, K. Czamara, M. Z. Pacia, K. Majzner, K. Kochan, A. Kaczor, M. Baranska and K. Malek, "Raman and infrared spectroscopy of carbohydrates: A review," *Spectrochimica Acta Part A: Molecular and Biomolecular Spectroscopy*, vol. 185, pp. 317-335, 2017.

[74] U. P. Andley, "The Lens Epithelium: Focus on the expression and function of the alpha-crystallin chaperones," *The international journal of biochemistry & cell biology*, vol. 40, no. 3, pp. 317-323, 2008.

[75] R. J. W. Trusott and M. G. Friedrich, "Molecular Processes Implicated in Human Age-Related Nuclear Cataract," *Investigative Ophthalmology & Visual Science*, vol. 60, no. 15, pp. 5007-5021, 2019.

[76] J. Bilbao and A. d. Miguel, "Estimation of UV-B irradiation from total global solar meteorological data in central Spain," *Journal of Geophysical Research: Atmospheres*, vol. 115, no. D1, 2010.

[77] S.-Y. Lin, C.-J. Ho and M.-J. Li, "UV-B-induced secondary conformational changes in lens α-crystallin," *Journal of Photochemistry and Photobiology B: Biology*, vol. 49, no. 1, pp. 39-34, 1999.

[78] A. G. Abraham, C. Cox and S. West, "The Differential Effect of Ultraviolet Light Exposure on Cataract Rate across Regions of the Lens," *Investigative Ophthalmology & Visual Science*, vol. 51, no. 8, pp. 3919-3923, August 2010.

[79] J. D'Orazio, S. Jarretty, A. Amaro-Ortiz and T. Scott, "UV Radiation and the Skin," *International Journal of Molecular Sciences*, vol. 14, no. 6, pp. 12222-12248, 7 June 2013.

[80] A. Spector and W. H. Garner, "Hydrogen peroxide and human cataract," *Experimental Eye Research*, vol. 33, no. 6, pp. 673-681, 1 December 1981.